INVESTIGATING THE STRUCTURAL RESPONSE OF LAMINATED GLASS PLATES UNDER RIGID BODY IMPACT LOADS

T. W. M. C. Wanigasooriya

238059G

Master of Science (Major Component Research)

Department of Civil Engineering
Faculty of Engineering

University of Moratuwa
Sri Lanka

May 2025

INVESTIGATING THE STRUCTURAL RESPONSE OF LAMINATED GLASS PLATES UNDER RIGID BODY IMPACT LOADS

T. W. M. C. Wanigasooriya

238059G

Thesis/Dissertation submitted in partial fulfilment of the requirements for the degree

Master of Science

Department of Civil Engineering

Faculty of Engineering

University of Moratuwa

Sri Lanka

May 2025

DECLARATION

I declare that this is my own work, and this thesis/dissertation does not incorporate without acknowledgement any material previously submitted for a degree or diploma in any other University or Institute of higher learning and to the best of my knowledge and belief it does not contain any material previously published or written by another person except where the acknowledgement is made in the text. I retain the right to use this content in whole or part in future works (such as articles or books).

Signature: Date: 24/12/2025

The above candidate has carried out research for the PhD/MPhil/Masters thesis/dissertation under my supervision. I confirm that the declaration made above by the student is true and correct.

Name of Supervisors: Dr. H. G. H. Damruwan

Dr. K. Baskaran

Signature of the Supervisors: Date:

Dr. H. G. H. Damruwan 24/12/2025

24/12/2025

Dr. K. Baskaran

DEDICATION

To my loving parents and little brother. Thank you for your endless love, strength, patience, and constant support. This thesis is a reflection of your faith in me, and I dedicate it to you with all my heart.

ACKNOWLEDGEMENT

There are many people who have been a constant source of encouragement and support throughout my MSc journey. While it is impossible to name everyone, a few individuals deserve special recognition for their contributions.

First and foremost, I would like to express my deepest gratitude to my supervisors, Dr. H. G. H. Damruwan and Dr. K. Baskaran, for their unwavering guidance, and encouragement. Dr. H. G. H. Damruwan has been a mentor to me since my undergraduate days and also supervised my undergraduate research. His patient mentoring has played a crucial role in shaping both this work and my development as a researcher. I am equally thankful to Dr. K. Baskaran for his generous support and for consistently encouraging me to challenge myself and grow academically. Their combined expertise, constructive feedback, and sincere dedication were instrumental in the successful completion of this thesis.

I would also like to express my sincere thanks to Dr. Lakshitha Fernando for his invaluable feedback during each progress review. His thoughtful comments and suggestions have added great value to the development of this thesis.

Special appreciation goes to Eng. Chathura Jayaweera and Eng. Pasindu Meddage for their technical support and valuable discussions, which helped me navigate challenges during the research process.

I would also like to acknowledge, with deep respect, all my teachers from preschool through school, and the lecturers at the University of Moratuwa, Sri Lanka. Their guidance and dedication laid the educational foundation on which this academic journey was built, and I am truly grateful for the role they played in shaping my early development.

I am also thankful to all my colleagues and friends who supported me along the way. Your companionship and encouragement made this journey more manageable and meaningful.

Finally, and most importantly, I extend my heartfelt gratitude to my parents and my little brother. Their unconditional love, patience, and faith in me have been the foundation of my academic pursuits. This accomplishment is as much theirs as it is mine.

ABSTRACT

Laminated glass (LG) plays a vital role in impact-resistant glazing systems aimed at safeguarding against severe loads from events like hurricanes, windstorms, forced entries, air blasts, and ballistic threats. Nevertheless, our understanding of its resistance to perforation when struck by large rigid missiles is limited, as most research has centred on small missile impacts due to the high cost and complexity of full-scale large rigid body impact testing on LG. Although the response of laminated float glass to impact has been examined, much of this research has concentrated on static or quasi-static parameters. There has been limited exploration into how the rate of loading affects the prediction of LG's impact resistance under dynamic scenarios. Currently, there are no established guidelines for evaluating LG's resistance to rigid projectiles while considering the separate influences of projectile mass, impact velocity, and contact area. This research aims to fill these gaps by calibrating the Johnson-Holmquist Ceramic (JH-2) parameters for LG, utilizing a meta-analysis of existing studies to enhance the precision of impact simulations. A finite element (FE) model is developed to anticipate how LG panels with polyvinyl butyral (PVB) interlayers respond to large missile impacts. This model is validated using experimental data from the literature, carried out in accordance with ASTM standards. The study further develops the numerical model to create perforation vulnerability curves for LG panels based on 270 different impact scenarios. It reveals that increased interlayer thickness improves perforation resistance. Unlike earlier numerical analyses, this work incorporates silicone sealants between glass and aluminium frames, reducing peak stress by more than 90%, delaying stress peaks, redistributing the impact energy, and decreasing the number of cracks at panel edges. Furthermore, it identifies that impact momentum alone is insufficient to predict perforation resistance, emphasizing the separate effects of projectile mass, impact velocity, and projectile contact area. These findings contribute to a structured approach for assessing LG performance under high-strain impact conditions, closing the gap between theoretical and practical applications, and guiding the design of safer, more effective impact-resistant glazing systems.

Keywords: Laminated glass (LG); Johnson-Holmquist ceramic (JH-2) model; Perforation vulnerability curves; Large missile impact; Protective glazing systems; Finite element modelling; Glass fracture mechanics

TABLE OF CONTENTS

LIST OF FIGURES

LIST OF TABLES

LIST OF ABBREVIATIONS

Abbreviation	Description
LG	Laminated Glass
PVB	Poly-vinyl Butyral
EVA	Ethylene-vinyl Acetate
FE	Finite Element
JH-2	Johnson-Holmquist Ceramic Model
ASTM	American Society for Testing and Materials
HEL	Hugoniot Elastic Limit
EOS	Equation of State
SPH	Smooth Particle Hydrodynamics
SGP	SentryGlas Plus
CTS	Cyclone Testing Station
AS/NZS	Australian Standard/ New Zealand Standard
SHPB	Split Hopkinson Pressure Bar
MAPE	Mean Absolute Percentage Error
R^2	Coefficient of Determination
RMSE	Root Mean Square Error

CHAPTER 1

INTRODUCTION

1.1 Background

In recent decades, laminated glass (LG) has evolved from a safety feature in automotive windshields to a critical structural component in architectural and protective applications. Its growing prevalence in modern buildings, façades, curtain walls, and security infrastructure stems from its unique ability to combine transparency with enhanced safety, structural performance, and energy absorption [1]. These attributes make LG indispensable in structures exposed to severe environmental and man-made hazards.

LG typically consists of two or more glass plies bonded by polymeric interlayers such as polyvinyl butyral (PVB), ethylene-vinyl acetate (EVA), or ionoplasts like SentryGlas Plus (SGP). The interlayer plays a pivotal role in maintaining the structural coherence of the glass after fracture, preventing disintegration, and reducing the risk of injury from flying glass shards [2], [3]. This composite behaviour ensures that the broken glass adheres to the interlayer, maintaining a barrier against further intrusion and external exposure, which is particularly important in applications requiring blast resistance, forced entry delay, or windborne debris mitigation.

Advancements in interlayer technologies and composite glass mechanics have enabled LG to resist not only service-level loads but also extreme transient events, including shock waves, impulsive loads, and debris impacts [4]. As a result, LG is increasingly incorporated into buildings located in cyclone-prone regions, critical infrastructure, embassies, transportation hubs, and high-security zones, where performance under sudden, high-energy impacts is vital. In addition to its functional advantages, LG also supports aesthetic and sustainability goals. It supports architectural transparency, noise attenuation, and solar control, aligning with modern green building initiatives. Furthermore, its ability to be customized in terms of thickness, layer configuration, and boundary conditions allows structural engineers to tailor glazing systems for specific risk levels and design constraints.

Given these expanding applications, understanding the structural response of LG under extreme loading conditions has become an essential area of inquiry. The increasing reliance on performance-based design principles and the push towards resilient infrastructure demand accurate and predictive tools to evaluate LG systems under realistic impact scenarios. This study is situated within that evolving context, one that recognizes LG not merely as a glazing option, but as a structural safety element critical to occupant protection, façade resilience, and system-level performance in adverse environments.

1.2 Problem Statement

Although LG is a well-established solution in impact-resistant glazing, its perforation resistance under large rigid missile impacts remains poorly understood. Most of the prior research focuses on small projectiles and quasi-static loading conditions, thereby failing to capture the complex dynamic response observed during real-world events such as hurricanes, explosions, or high-speed debris strikes. Moreover, the existing experimental databases are sparse due to the high cost, safety risks, and logistical challenges of conducting full-scale impact tests. As a result, designers lack a validated and systematic framework to assess the perforation resistance of LG in scenarios that simulate extreme real-world events, including windborne debris during cyclones, blast waves, and forced entry attacks.

A key issue is the widespread use of static and quasi-static material parameters, which do not account for the dynamic behaviour of glass and interlayer materials under high strain rates. This simplification can lead to significant inaccuracies in predicting the structural response of LG, particularly under explicit impact conditions that involve high strain-rate loading. Therefore, it becomes imperative to develop a methodology that incorporates appropriately calibrated dynamic material properties for both glass and polymer interlayers to enhance the predictive accuracy of numerical simulations.

Additionally, most prior numerical studies have focused on steel ball impacts [5] or automotive crash simulations [6], while systematic research on wood block impacts, which represent standardized large missile scenarios [7], [8], [9], [10], remains scarce. Although Zhang et al. [3] attempted to model large projectile impacts experimentally and numerically, their finite element (FE) model did not consider the silicone sealant used between the glass and the supporting frame. Silicone sealants serve a critical role in energy redistribution and stress attenuation at the panel boundaries, yet their mechanical influence under impact conditions is still poorly understood.

Furthermore, limitations exist in the Johnson-Holmquist Ceramic (JH-2) material model parameters used in earlier simulations, particularly in the determination of Hugoniot Elastic Limit (HEL), which is vital for capturing glass behaviour under high-pressure dynamic conditions. Subsequent refinements by Zhang et al. [11] and Zhou et al. [12] introduced enhanced JH-2 parameters including revised tensile strength and pressure coefficients, significantly improving the model's fidelity. Building upon these developments, the present study conducts a systematic meta-analysis and calibration of the JH-2 model, ensuring more accurate and realistic simulations of LG panels under standardized wood block projectile impacts.

This research intends to address these challenges by developing a robust FE model incorporating dynamically calibrated JH-2 material parameters, realistic projectile characteristics, and boundary condition modelling including silicone sealants.

1.3 Aim and Objectives

The main aim of this thesis is to develop and validate a comprehensive finite element (FE) modelling framework for predicting the impact response of LG and use it to assess the impact performance of LG under large rigid body impacts. This aim will be achieved by undertaking the following research objectives.

- Develop a comprehensive FE model with suitable material parameters and contact types.
- Validate the FE model using past experimental results, including centre deflection time-history curves, maximum strains, and crack patterns.
- Examine the effects of impact velocity, impactor mass and geometry, and thickness of interlayer under rigid body impacts.
- Develop perforation vulnerability curves based on the interlayer thickness, impactor mass and contact surface area.

1.4 Research Scope and Limitations

This study is primarily concerned with investigating the structural response of LG panels subjected to large rigid body impacts, specifically focusing on timber projectile impacts as defined in internationally recognised standards such as ASTM E1996-23 [9] and AS/NZS 1170.2:2011 [13]. The research centres on large missile scenarios rather than small projectile or quasi-static conditions, with the aim of contributing to performance-based design frameworks for glazing systems in impact-prone environments. The LG configurations analysed in this study utilise PVB as the interlayer material due to its widespread adoption in architectural applications and its viscoelastic behaviour under dynamic loading.

A high-fidelity three-dimensional (3D) FE model is developed using LS-DYNA commercial software package, employing the explicit dynamic formulation to simulate the nonlinear behaviour of LG under high-strain-rate conditions. The numerical modelling methodology captures both the elastic and damage-phase responses of the LG panels across a range of impact parameters, including variations in impact velocity, glass ply thickness, interlayer thickness, impactor mass, and impactor contact geometry. These simulations provide insights into perforation behaviour and energy dissipation mechanisms, contributing to a better understanding of the failure thresholds in LG systems.

Despite its comprehensive scope, the study is limited to rigid wood block projectiles and exclude other impactor types such as metallic or deformable bodies. In addition, the material models, although calibrated against experimental data, do not account for temperature-dependent behaviour or long-term environmental degradation. The boundary conditions are idealised based on standard laboratory test setups. While efforts have been made to reflect realistic support conditions, actual field installations may involve additional complexities that are not fully represented in this study. Although LS-DYNA provides robust modelling capabilities, its high computational cost imposes practical limitations on the number of parameter combinations that can be explored. As a result, the analysis focuses on a selected range of representative scenarios.

1.5 Significance and Innovation of Research

LG plays a vital role in structural and architectural applications, particularly where occupant safety and post-fracture integrity are critical. Its superior performance compared to monolithic glass has led to widespread adoption in buildings exposed to blast loads, forced entry attempts, and windborne debris impacts. However, the structural response of LG under impact loads involves complex interactions between the brittle glass plies and the viscoelastic interlayer, which remain not fully understood. Gaining a deeper understanding of these mechanisms is essential for designing glazing systems that are both safe and structurally efficient.

In extreme weather scenarios such as hurricanes and tornadoes, debris impact can lead to catastrophic failure of glazing systems, causing significant risk to life and property. Accurate prediction of such impact responses is essential for the development of effective mitigation strategies. Although experimental testing remains important for performance evaluation, it is often associated with high financial, logistical, and safety demands. Full-scale impact tests require specialized facilities and are constrained by the range of conditions they can feasibly replicate.

This research addresses these challenges by developing high-fidelity FE models that simulate the impact behaviour of LG panels under large rigid body impacts. The numerical approach adopted in this study provides a cost-effective and flexible alternative to large-scale experimental programs, enabling the analysis of a wide range of parameters such as projectile mass, velocity, contact area, glass ply thickness, and interlayer thickness. The validated FE models can serve as powerful predictive tools for performance-based design and will contribute to enhancing the safety and resilience of glazing systems in hurricane-prone regions. Moreover, the findings of this study offer valuable insights for refining existing building codes and standards related to hurricane-resistant glazing systems.

1.6 Thesis Organization

This thesis consists of five chapters as follows:

Chapter 1 contains an introduction of the research explaining background study, research problem, aim and objectives, scope of the research, importance of the study, and thesis outline.

Chapter 2 presents a review of relevant literature from previous years. It consists with structural and safety aspects of LG, concepts of impact loads, impact testing standards, experimental studies and numerical studies conducted related to LG under impact loads, and finally pointing out the research gaps in current literature.

Chapter 3 delivers the research methodology carried out in the current study including the development of the FE model, mesh sensitivity analysis, validation of the modelling techniques with experimental results.

Chapter 4 describes the effects of silicone sealant, aluminium frame and PVB interlayer when subjected to impact loads, and development of the perforation vulnerability curves to assess the performance of LG under impact loads.

Chapter 5 concludes the thesis by summarising the current research process, main findings of the research, and recommendations for the future research.

CHAPTER 2

LITERATURE REVIEW

2.1 Introduction

This chapter begins with an introduction (Section 2.1), which explains the content of each section briefly. Section 2.2 presents a detailed overview of LG as a structural and safety material. This includes its composition, mechanical properties, fracture characteristics, and common applications in architectural, automotive, and protective glazing systems. The section establishes a fundamental understanding of LG necessary to contextualize its behaviour under impact.

Section 2.3 describes the nature of impact loads, providing an overview of different impact velocity ranges, their classifications, and relevance to structural applications. It also introduces the fundamental energy transfer mechanisms and key parameters that govern impact behaviour, such as impact velocity, mass, angle, and projectile geometry.

Section 2.4 reviews experimental studies on LG under impact loads. It begins with an overview of established impact testing standards and continues with a critical assessment of laboratory investigations, highlighting various testing methods, observed damage mechanisms, and the influence of material and impactor parameters on performance outcomes. Section 2.5 examines numerical modelling approaches used to simulate the impact behaviour of LG. This section discusses FE techniques, including the application and calibration of the Johnson-Holmquist Ceramic (JH-2) model. It also identifies key limitations in previous modelling practices.

Finally, Section 2.6 summarises the key gaps and limitations identified throughout the literature, which serve as the motivation for the present study. The review highlights the need for accurate dynamic modelling, and inclusion of large projectile impacts. These observations establish a strong foundation for the development of the research methodology in the subsequent chapter.

2.2 Laminated Glass as a Structural and Safety Material

2.2.1 Architectural and Structural Relevance of Laminated Glass

Glass is one of the most widely utilized materials in modern architecture for its transparency, aesthetic appeal, and ability to create open, light-filled spaces. Its presence in façades, canopies, railings, and skylights contributes significantly to both the visual and functional performance of modern buildings [14]. However, these glass elements are frequently exposed to demanding service conditions, including both natural hazards such as high wind loads, hail, and earthquakes, and manmade threats like accidental impacts, forced entry attacks, and blasts.

Traditional monolithic float glass, while visually desirable, is inherently brittle and prone to sudden, dangerous fragmentation under extreme loads. Upon failure, it shatters into sharp, high-velocity shards that pose significant injury risks and can no longer offer barrier protection. These vulnerabilities have led to the widespread adoption of more robust alternatives in critical applications, leading to the widespread adoption of LG systems. Due to its superior safety performance, LG is widely used in applications that demand resistance to impact, structural integrity after breakage, and occupant protection [1], [14], [15], [16]:

- Automotive windshields: Ensures passenger safety by maintaining integrity during crashes or debris impacts.
- Balustrades and Railings: Prevents falls while resisting accidental impacts in residential and commercial buildings.
- Glass Floors and Stairs: Supports pedestrian loads and withstands dynamic forces in modern architectural spaces.
- Skylights and Canopies: Protect against falling objects and weather-induced damage.
- Security and bullet-resistant glazing: Provides resistance to forced entry and ballistic threats in high-risk environments.
- Curtain walls and Façades: Enhances building safety during storms, blasts, and seismic events.
- Sports arenas: Serves as protective barriers against high-speed balls or pucks.
- Museums and Galleries: Offers both transparency and protection for valuable artifacts.

These diverse use cases illustrate the critical role of LG in environments where structural demands and safety considerations intersect.

2.2.2 Concept and Composition of Laminated Glass

LG is a composite safety material formed by bonding two or more layers of glass using transparent polymer interlayers under controlled heat and pressure [15], [17]. This configuration allows the panel to retain its integrity upon fracture, with the interlayer acting as a binding medium that holds the broken shards together and prevents disintegration (see Fig. 2.1). The interlayer not only enhances post-breakage behaviour but also contributes to shear coupling between the glass plies, vibration damping, and energy absorption during impact [18], [19]. LG thus serves as both a structural and safety component, effectively mitigating risks associated with fragmentation while improving resistance to various loading types.

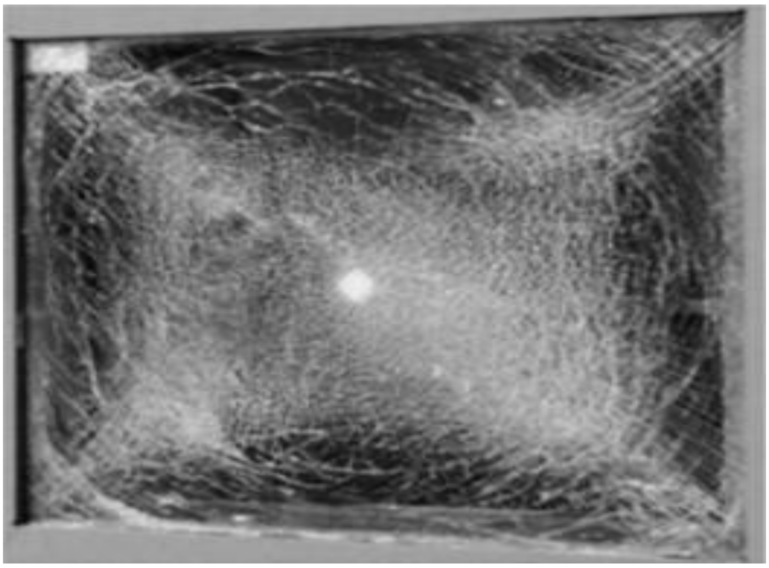

Fig. 2.1: Fractured laminated glass panel subjected to blast load [20]

Soda-lime silicate glass is the most commonly used material in architectural applications. Table 2.1 exhibits the physical and mechanical properties of Soda-lime silicate glass.

Table 2.1: Physical and mechanical properties of soda-lime silicate glass [21], [22]

Properties	Value
Density	2500 kg/m^3
Young's modulus	70000 MPa
Poisson's ratio	0.23
Shear modulus	28455 MPa
Hardness	6 GPa
Compressive strength	880-930 MPa
Tensile strength	30-90 MPa
Bending strength	30-100 MPa

In modern glass industry, soda-lime silicate glass is classified into three main types based on heat treatment: annealed glass (AN), heat-strengthened glass (HS), and fully tempered (toughened) glass (FT). These types differ in their strength and safety characteristics due to variations in the manufacturing process, particularly the cooling rate after heating. Table 2.2 shows the ultimate tensile and compressive stress for all three glass types [22].

Table 2.2: Tensile and compressive strengths of glass types [22]

Glass type	Surface Compression (MPa)	Tensile Strength (MPa)		Compressive Strength (MPa)
		Long Term	Short Duration (Blast/ High velocity impact)	
AN	0	45	80	n/a
HS	24-69	70	168	25 – 40
FT	>69	120	200	69

The performance of LG depends significantly on the materials used in its construction:

- Glass Plies:
    - Annealed Glass (AN): Standard float glass with minimal internal stresses.
    - Heat-Strengthened Glass (HS): Stronger than AN, with better resistance to thermal stress and impact.
    - Tempered Glass (FT): Four to five times stronger than AN; shatters into small, blunt pieces for safety.
- Polymer Interlayers:
    - Polyvinyl Butyral (PVB): Most widely used due to its high adhesion, clarity, and flexibility.
    - Ethylene-Vinyl Acetate (EVA): Offers improved moisture resistance and durability.
    - Ionoplast (e.g., SGP): Delivers enhanced structural stiffness and UV resistance.

Each glass and interlayer type provides different mechanical and durability properties, influencing the overall response of the LG panel under impact conditions. The fragmentation pattern upon failure varies significantly between glass types and is an essential aspect of safety design (see Table 2.3).

LG, when incorporating these based materials, benefits from the interlayer's ability to retain fragments and mitigate the dangers of glass ejection, making it particularly effective in impact-prone applications.

Table 2.3: Failure patterns of different glass types [23]

Glass type	**AN**	**HS**	**FT**
Failure pattern			
Description	Breaks into large, sharp shards that can cause severe injuries (not considered as safety glass).	Produces larger fragments but maintains partial resistance to disintegration (not considered as safety glass).	Shatters into small, blunt pieces and often vacates the frame reducing lacerating risk (considered as safety glass).

2.3 Nature of Impact Loads

Impact loading is a critical factor in structural design across a broad spectrum of industries, including construction, automotive, military, aerospace, offshore, naval, and sports engineering [24]. The complexity of these loading conditions arises from the sudden application of force over a short time interval, often resulting in localised damage, high strain-rate effects, and dynamic material responses. Understanding the nature, classification, and mechanisms of impact is essential for accurate modelling, experimental testing, and performance evaluation of materials and structural systems such as LG.

Impact events are broadly classified by velocities, each associated with distinct mechanical phenomena, testing methods, and applications. Backman and Goldsmith [25], Ball and McKenzie [26], and Børvik [27] proposed a widely accepted categorization based on projectile velocity, which continues to inform both experimental research and numerical modelling frameworks (see Table 2.4).

While this classification provides a structured understanding, alternative definitions have been proposed in literature. Zukas [28] suggests defining low-velocity impacts as those below 250 m/s and ordnance-level impacts as ranging from 500 to 2000 m/s. Such variation highlights the dependency of classification on specific industry requirements and test methods. In more recent research, when investigating the impact response of structural components such as LG, researchers have increasingly prioritized practical, real-world scenarios over strict adherence to predefined velocity classifications such as those presented in Table 2.4.

At the onset of impact, the kinetic energy of the projectile is transferred to the target structure, initiating a range of material responses. The initial contact triggers a complex redistribution of energy into various forms, including elastic vibration, plastic deformation, fracture energy, and localised heating. Corran et al. [29] characterised this initial interaction by the following response mechanisms in the target material:

- Elastic wave propagation and energy dissipation at supports or clamped boundaries
- Plastic deformation due to stretching, bending, and shear effects
- Localised plastic flow near the impact point

The extent and dominance of each mechanism depend heavily on the impact energy and the nature of both the projectile and target materials.

Table 2.4: Different velocity ranges and representative test methods and applications

Velocity Range	**Impact test equipment**	**Material test method**	**Typical applications**
Low velocity 0 – 50 m/s	- Drop hammer - Pneumatic acceleration	- Quasi-static test - Hydraulic	- Dropped objects - Vehicle impact - Ship collision
Sub-ordnance 50 – 500 m/s	- Compressed air gun - Gas gun	- Pneumatic - Hydraulic - Taylor impact test - Split Hopkinson Pressure Bar (SHPB) test	- Free falling bombs and missiles - Nuclear industry - fragments due to bomb explosions - hurricane debris
Ordnance 500 – 1300 m/s	- compressed gas gun - powder gun	- Taylor impact test - SHPB test	- Military-grade projectiles and weapon testing
Ultra-ordnance 1300 – 3000 m/s	- Powder gun - Two-stage light gas gun	- Taylor impact test - Plate impact test	- Advanced military and ballistic research
Hypervelocity 3000 – 12000 m/s	- Two-stage light gas gun	- Plate impact test	- Spacecraft shielding - Orbital debris protection
Highest velocity >12000 m/s	n/a	n/a	- Theoretical or specialised simulations

Impact behaviour is highly sensitive to a number of interacting parameters that define the conditions and consequences of the event. The key influencing factors identified by Backman and Goldsmith [25] and Zukas [28] include:

- Impact velocity, which directly governs kinetic energy

- Impact angle, influencing the direction and distribution of stresses
- Material properties of the target, such as strength, ductility, and failure modes
- Material properties of the projectile, including stiffness and fracture behaviour
- Projectile geometry, affecting penetration, contact area, and stress concentration
- Trajectory and contact location, which determine impact severity and energy dispersion

These variables contribute to a highly nonlinear and rate-sensitive structural response, which must be captured in both experimental and numerical studies.

In real-world scenarios, impacting objects often possess irregular or semi-regular contact geometries, reflecting natural or engineered forms. However, for the purpose of numerical and experimental analysis, researchers have adopted idealised projectile shapes that simplify the analysis of impact phenomena. Studies by Goldsmith [30], Zhang et al. [3], Timmel et al. [6], Hála et al. [31], and Zemanová [32], [33] have utilized a range of projectile shapes, including flat-nosed, hemispherical-nosed, conical, ogive-nosed, and cylindrical configurations (see Fig. 2.2). These idealisations are instrumental in advancing the understanding of penetration resistance and dynamic failure processes in target objects.

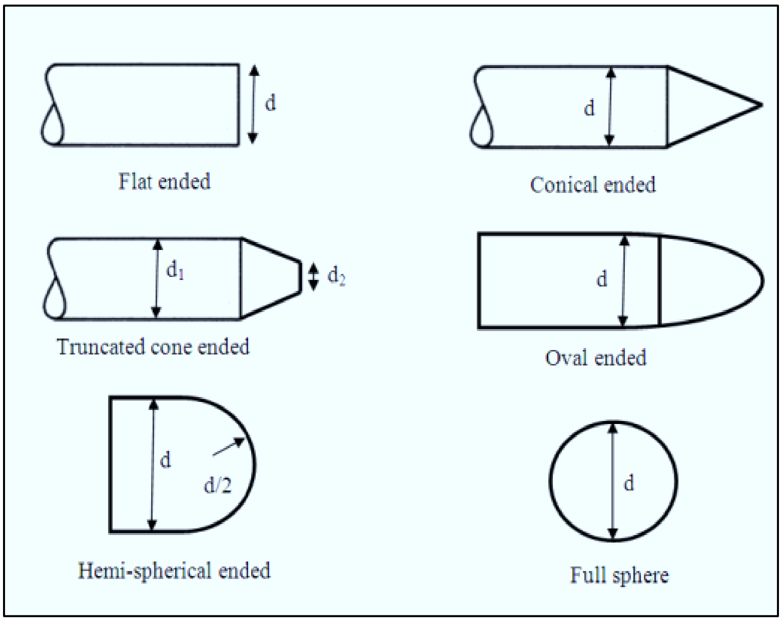

Fig. 2.2: Different projectile contact shapes [3], [6], [21], [31], [33]

2.4 Experimental Investigations on Impact Performance of LG

2.4.1 Impact Testing Standards for LG under Projectile Impacts

The impact resistance of LG is a critical performance parameter, particularly due to its inherent vulnerability to sudden and high intensity loading scenarios [34], [35], [36], [37]. While the interlayer in LG significantly enhances post-fracture integrity, rigid body impacts, especially those involving large projectiles, continue to present a considerable challenge [36], [37].

To address these challenges, a series of design codes and standards have been developed to specify the types of impactors and testing procedures necessary to evaluate the performance of LG panels. Two representative missile types are widely recognised: a timber block and a steel ball. Specifically, the Australian/ New Zealand Standard [7] prescribes the use of:

- A timber block with a normal mass of 4 kg, and cross-sectional dimensions of 100 mm × 50 mm for large missile impacts.
- A spherical steel ball of 8 mm diameter and approximately 2 g mass for small missile impacts, intended to simulate debris like gravel or steel fragments.

In addition, the U.S. Defence Civil Preparedness Agency (DCPA) [10] established an early precedent by proposing a 7 kg, 50 mm × 100 mm timber rod to set impact resistance criteria for tornado shelters in educational and residential buildings.

Standards such as ASTM E1886-19 [8], ASTM E1996-23 [9], and earlier versions of AS/ NZS 1170.2 [13] have further refined these specifications. They generally require protective glazing systems to resist the impact of a 4 kg wooden block travelling at 15 m/s, replicating hurricane-induced debris impacts. More recently, AS/NZS 1170.2:2021 [7] allows the impact velocity to be adjusted based on design wind speeds, specifying 0.4 times the design wind speed for horizontal trajectories and 0.1 times the design wind speed for vertical trajectories. Under extreme wind conditions, projectile velocities can exceed 40 m/s, significantly intensifying the demands placed on glazing systems. In 2017, the Cyclone Testing Station (CTS) at James Cook University introduced the "Technical Note No. 04" offering additional procedural recommendations for impact testing. The CTS guidelines emphasize the necessity to test at multiple panel locations, including the geometric centre, interface corners, and edges to capture a more comprehensive understanding of glazing performance. However, the document does not prescribe specific tolerance levels for these impact locations, introducing some variability in test interpretations [38].

The ASTM E1886-19 [8] standard provides a detailed methodology for specimen mounting, missile impact, cyclic pressure loading, observation, and results interpretation. It also specifies three types of missile propulsion devices:

- Large missile air cannon,
- Bungee test apparatus,
- Small missile air cannon.

In addition to this, ASTM E1996-23 [9] establishes some set of guidelines to conduct the impact tests which are given in ASTM E 1886-19 [8] and criteria for evaluating the performance of building envelopes.

2.4.2 Experimental Studies on Impact Behaviour of LG

The impact performance of LG is governed by a complex interplay of material properties, impact conditions, and boundary configurations. Early studies by Backman and Goldsmith [25] and Zukas [28] identified several critical factors that significantly influence the structural response of LG under impact events. Among these, the impact velocity plays a decisive role in determining the magnitude of energy transfer and the extent of induced damage. Impactor mass is another major determinant, with heavier projectiles imparting greater momentum and energy, thus leading to more severe structural responses. The angle of impact is also significant, as oblique impacts can result in asymmetric stress distributions and complex fracture patterns compared to normal impacts. Furthermore, the geometry of the impacting surface and the thickness of the glass plies and interlayer materials critically affect the modes of energy absorption, crack initiation, and post-fracture behaviour of LG systems.

To understand these interactions, a variety of experimental methods have been developed over the decades. These include quasi-static testing for low-speed applications, drop weight impact tests simulating free-falling objects, pendulum tests often used in architectural applications, gas-gun tests for controlled high-velocity impacts, and Split Hopkinson Pressure Bar (SHPB) tests for capturing material responses at high strain rates. Among these, drop weight impact testing has emerged as one of the most common approaches to evaluate both monolithic and laminated glass behaviour. Studies by Belingardi [39], Aretxabaleta [40], Liu and Liaw [41], and Zhu and Chai [42] have all employed variations of the drop weight methodology to examine the dynamic performance of LG panels. Within laboratory environments, this method is also commonly referred to as drop-tower testing, ball-drop testing, or tool-drop testing, depending on the specific apparatus and test configuration.

A number of significant experimental investigations have shaped current understanding of LG impact response. Langitan and Lawn [43], Wiederhorn and Lawn [44], and Kirchner and Gruver [45] provided early insights into fracture mechanisms in glass materials under localised impact loads. Later, Ball and McKenzie [26] and Ball [46] extended these studies to include LG systems, observing the propagation of fracture patterns and the influence of stress waves generated by projectile impacts. Grant et al. [47] and Grant and Cantwell [48] studied the impact resistance of automotive LG panels by varying inner and outer ply thicknesses while maintaining a constant PVB interlayer thickness, providing valuable data on the role of glass composition in impact performance.

Further investigations into LG panels subjected to drop weight impacts were conducted by Shutov et al. [49], who employed a 4.11 kg impactor dropped from various heights (3.5 m, 6.5 m, and 9.5 m) on 500 mm × 500 mm LG specimens. Their research revealed characteristic fracture patterns and energy dissipation behaviours, contributing important experimental benchmarks for model validation. Complementarily, Ball [46] utilised a 5 mm diameter spherical steel projectile to study the stress-induced fracture propagation on LG plates under velocities ranging from 10 m/s to 100 m/s, observing distinct cone-shaped and star-shaped fracture patterns depending on the impact velocity and glass configuration. One notable study conducted by Zhang et al. [3] examined the debris impact resistance of LG windows. Utilizing a 4 kg timber projectile with a flat contact surface measuring 100 mm × 50 mm and an impact velocity of 15 m/s, Zhang's experiments documented central displacement histories, fracture propagation patterns, and the behaviour of glass fragment ejection during impacts. These findings provided further clarity of LG behaviour under debris impact loading conditions. Fig. 2.3 and Fig. 2.4 show two different fracture patterns of LG which are subjected to two different impactors (steel ball and timber block) with different impact conditions.

Fig. 2.3: Fracture patterns of LG plates under steel ball impact conducted by Shutov et al. [49]

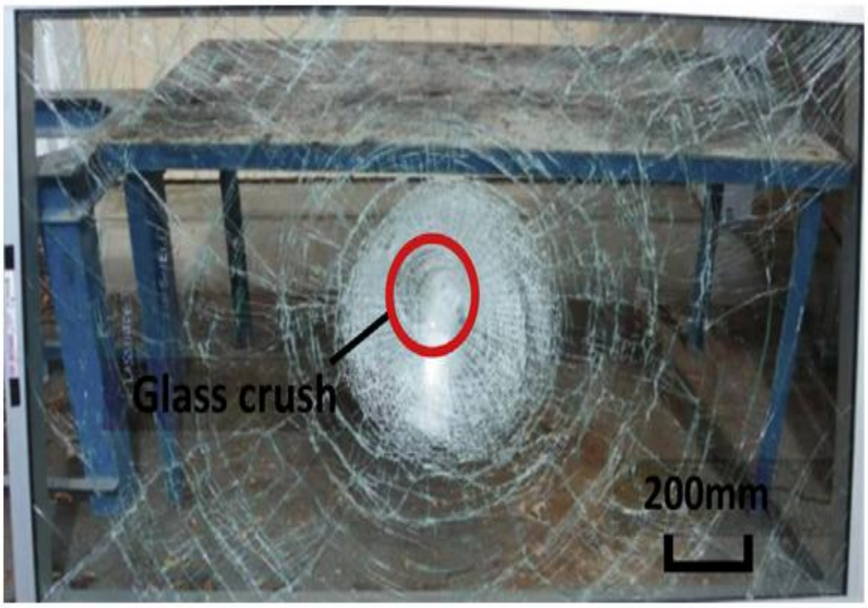

Fig. 2.4: Fracture patterns of LG plates under wood block impact conducted by Zhang et al. [3]

The influence of impactor properties, particularly mass and size, has been rigorously explored by researchers such as Beason et al. [50] and Harris [51]. Beason et al. [50] concluded that the size of the impacting missile critically influences glass failure, while Harris [51], through testing over 200 glass samples, determined that projectile mass is the most important factor governing damage severity. In the context of timber projectile impacts, Bole [52] demonstrated that even with identical kinetic energies, different projectile masses can produce different breakage patterns in annealed, heat-strengthened, and tempered glass panels. Projectile geometry also plays a fundamental role in determining impact outcomes. A range of geometries, including spherical, hemispherical, flat blunt, cylindrical, and conical shapes, have been systematically studied by Shutov et al. [49], Liu and Liaw [41], Zhu and Chai [42], Kishi and Bhatti [53], Liu et al. [54], and Dhakal et al. [55]. These studies underscore that impactor shape affects the contact area, stress concentration, penetration behaviour, and overall fracture mechanisms during impact events.

Experimental investigations have evaluated a variety of response parameters to characterise the impact performance of LG. These include measurements of impact force, displacement histories, acceleration profiles, absorbed and residual energy, impact velocity at breakage, damage morphology, contact duration, post-impact residual velocities in cases of penetration, and the extent of fragmentation and interlayer delamination. Although experimental research has greatly advanced the understanding of impact-induced damage in LG systems, significant gaps remain, particularly regarding the detailed mechanics of interlayer debonding, projectile-target interaction effects, and contact area evolution during high strain-rate events. These gaps highlight the continued need for advanced experimental and numerical studies, especially under conditions replicating large rigid body impacts.

While these testing methods indicated in Section 2.4.1 and 2.4.2 have significantly advanced the evaluation and certification of impact resistant glazing, several critical limitations should be noted. First, the cost associated with standard impact testing is substantial. LG panels are expensive, and the need for multiple specimens for rigorous testing imposes significant financial burdens on both commercial projects and academic research. University funding bodies and research institutions often face difficulties in conducting extensive experimental campaigns due to the prohibitive costs involved. Second, health and safety concerns are pronounced, especially at high impact velocities. Laboratory testing involving large rigid projectiles at velocities exceeding 30 – 40 m/s poses considerable risks to personnel and equipment, necessitating stringent safety precautions and specialised protective measures. Given these challenges, there is an increasing reliance on validated numerical models to supplement physical testing, offering a cost-effective, safer, and scalable means to predict the impact performance of LG systems under realistic conditions.

2.5 Numerical Studies on LG subjected to Impact Loads

While experimental studies have provided valuable insights into the structural response of LG under impact, large-scale physical testing remains prohibitively expensive, time-consuming, and often constrained by safety considerations. Consequently, numerical simulation methods have emerged as essential tools for evaluating the impact performance of LG systems under various loading conditions. Recent advances in computational mechanics have enabled detailed modelling of the brittle fracture behaviour of glass and the complex viscoelastic or viscoplastic response of polymer interlayers such as polyvinyl butyral (PVB) and SentryGlas Plus (SGP).

Two primary numerical approaches are employed when using FE analysis to simulate impact phenomena: the implicit and explicit FE methods. For dynamic problems such as high-velocity impacts, blast loads, shock waves, material erosion, and seismic analysis, the explicit method is considered the most appropriate due to its ability to handle severe nonlinearity, large deformations, and high strain rates [3], [22], [56], [57]. As a result, explicit dynamic simulations using commercial software packages such as LS-DYNA and ABAQUS have become standard practice in the impact analysis of LG systems.

Various numerical modelling methodologies have been explored to simulate the impact response of LG systems. Oda and Zang [58] utilized the discrete element method (DEM) to simulate the fracture behaviour of LG panels under steel ball impacts, demonstrating the potential of capturing fragmentation patterns. Liu and Liaw [41] adopted a three-dimensional (3D) finite element (FE) method to study the drop-weight impact behaviour of acrylic plates, discretising the structure with 8-node solid elements and applying a linear elastic material model. However, the damage behaviour was only inferred from sudden drops in the force-time curve, without detailed numerical representation of crack patterns. Expanding on these efforts, Zhu and Chai [42] proposed numerical models for both acrylic and polycarbonate plates subjected to low-velocity drop-weight impacts. Brittle damage models were assigned to acrylic plates, while ductile damage models were used for polycarbonate plates, allowing a comparative analysis of crack initiation and plastic deformation through contour plots, force-time, and force-displacement histories.

Flocker and Dharani [59], [60], [61] numerically examined the low-velocity impact response of LG panels subjected to missile impacts at 10 m/s. Using two-dimensional (2D) axisymmetric FE models, they evaluated stress distributions within the glass and interlayer, finding that increasing panel size and interlayer thickness significantly reduced maximum principal stresses in the non-impact side of the glass plate. However, the study did not investigate failure, penetration, or detailed damage patterns in LG plates. Timmel et al. [6] proposed a layered FE model for LG impact analysis, discretising the glass plies with shell elements and the interlayer with membrane elements. Their approach employed brittle cracking models for glass and hyperelastic models, such as Blatz-Ko and Mooney-Rivlin formulations, for the PVB interlayer. Wu et al. [62] further enhanced the impact simulations by applying the Johnson-

Holmquist (JH-2) model for glass plies and a linear isotropic plasticity model for the interlayer. Their study systematically investigated the effects of impact velocity, impactor size, and adhesion strength on LG performance. High-velocity impact events, such as those encountered in windshield applications, were addressed by Zang et al. [63] through a coupled Smooth Particle Hydrodynamics/Finite Element Method (SPH/FEM) approach. This allowed a more detailed depiction of material splashing and fragmentation, complementing earlier work by Timmel et al. [6] on the dynamic failure of LG.

Despite these advances, several limitations persist in existing numerical modelling approaches. Different software platforms, such as ABAQUS and LS-DYNA, employ distinct material models for glass fracture, such as the brittle cracking model in ABAQUS and the Johnson-Holmquist Ceramic (JH-2) model in LS-DYNA. However, the choice and calibration of material parameters remain critical challenges, as these properties often require extensive experimental validation for accuracy. In many cases, static or quasi-static material properties have been applied, leading to significant inaccuracies when predicting dynamic fracture behaviour under high strain-rate conditions.

The Johnson-Holmquist Ceramic (JH-2) material model, originally developed by Johnson and Holmquist [64], has become one of the most widely used constitutive models for simulating brittle materials like glass under high-strain rates. The JH-2 model incorporates the effects of strain rate sensitivity, pressure dependence, and progressive damage accumulation, making it highly suitable for modelling the dynamic fracture of glass. Holmquist et al. [65] provided the first parameter set for glass simulation, primarily targeting ballistic impact conditions. Subsequent studies refined these parameters to improve predictive accuracy for modern float glass compositions. Hidallana-Gamage et al. [66] proposed modifications by reducing the tensile strength component (T) while retaining the other JH-2 parameters. Zhang et al. [11] further refined the model by reducing tensile strength, pressure coefficients, Hugoniot Elastic Limit (HEL), and intact normalised strength constants (A and N), while increasing the strength parameter (C). Zhou et al. [12] built upon these refinements by slightly increasing the HEL and pressure component values compared to Zhang et al. [11], bringing them closer to Holmquist et al. [65] values, but maintaining reductions in normalized strength parameters. A summary of these parameter sets is presented in Table 2.5, with a detailed description and discussion of the parameters provided in Section 3.3.1.

Table 2.5: JH-2 parameters used by different researchers

	Parameters	Unit	Holmquist et al. [65]	Hidallana-Gamage et al. [22]	Zhang et al. [11]	Zhou et al. [12]
Strength Constants	A	-	0.93	0.93	0.75	0.70
	B	-	0.20	0.20	0.2	0.20
	C	-	0.003	0.003	0.035	0.035
	M	-	1.0	1.0	1.0	1.0
	N	-	0.77	0.77	0.72	0.72
	Max. tensile pressure (T)	MPa	150.0	60-65	27.8	27.8
	Max. norm. fracture strength (SFMAX)	-	0.5	0.5	0.5	0.5
	HEL	GPa	5.95	5.95	1.003	4.50
	HEL strength	GPa	4.54	4.5	0.334	3.15
	HEL pressure (PHEL)	GPa	2.92	2.92	0.78	2.40
Damage Constants	D1	-	0.043	0.043	0.043	0.043
	D2	-	0.85	0.85	0.85	0.85
Pressure Constants	K1	GPa	45.4	45.4	43.2	30.5
	K2	GPa	-138.0	-138.0	-67.2	-17.3
	K3	GPa	290.0	290	153.2	103.0
	Bulk (β/BETA)	-	1.0	1.0	1.0	1.0

Although significant progress has been made in numerical modelling, two major limitations persist. First, a widespread reliance on static or quasi-static material parameters undermines the predictive accuracy of simulations under high strain rate conditions typical of impact events. As a result, many models may not capture the reliable dynamic behaviour of LG plates. Second, the majority of previous numerical studies have focused on small projectile impacts, such as those caused by steel balls, or have addressed automobile crash scenarios. Systematic numerical investigations of large rigid body impacts, particularly those involving timber projectiles as specified in design standards like AS/ NZS 1170.2:2021 [7], ASTM E1886-19 [8], and ASTM E1996-23 [9], remain limited. Zhang et al. [3] made notable progress by developing a FE model for large projectile impacts on LG. However, the model did not account for the presence of silicone sealants at the glass-frame interface, an omission that could significantly affect boundary conditions and energy absorption characteristics during impacts (explained in Section 4.2). Furthermore, the JH-2 parameters employed lacked comprehensive calibration of HEL values, potentially affecting the accuracy of the simulated failure behaviour. Recognising these gaps, the present study undertakes a systematic calibration of the JH-2 model parameters based on a meta-analysis of previous research [11], [12], enhancing the reliability of simulations involving LG panels under large rigid wood block impacts. Additionally, this study incorporates the effect of silicone sealant and realistic boundary conditions, addressing previously neglected aspects and contributing to a more comprehensive understanding of LG behaviour under high-energy scenarios.

2.6 Limitations in Existing Research

This chapter has reviewed the existing literature on the structural and impact performance of LG, including its fundamental composition, mechanical behaviour, experimental investigations, and numerical modelling techniques. While considerable progress has been made in understanding LG under various impact scenarios, several critical limitations remain in the current body of research.

Experimentally, large-scale impact testing remains constrained by high costs, complex logistics, and safety concerns, especially when investigating full-scale glazing systems subjected to high-velocity or large-mass projectiles. Moreover, experimental studies have largely focused on specific configurations, often neglecting the combined effects of projectile geometry, contact location, material heterogeneity, and real-world boundary conditions. As a result, there remains a lack of comprehensive empirical data, particularly for full-size LG panels impacted by large rigid projectiles like timber blocks, which are used in standardised debris impact scenarios defined in AS/ NZS 1170.2:2021 [7] and ASTM E1996-23 [9].

In numerical analysis, FE modelling has emerged as a widely adopted tool for studying LG performance. Despite this progress, many existing models still rely on static or quasi-static material parameters that fail to capture the dynamic behaviour of glass and interlayer materials at high strain rates. Moreover, a majority of numerical studies have concentrated on small projectile impacts, such as steel balls, or have addressed automotive crash scenarios. Systematic research on large rigid body impacts, especially using timber projectiles as specified by debris impact standards, remains limited. Another persistent limitation lies in the treatment of boundary conditions. Many simulation models idealise glass support systems and omit the presence of critical components such as silicone sealants. These sealants not only provide weatherproofing and insulation but also influence stress distribution and energy dissipation during impact. Their exclusion reduces the realism of numerical predictions and restricts their applicability to real-world design scenarios. Although Zhang et al. [3] developed a FE model to simulate wood block impacts on LG, their approach did not incorporate sealant effects and was based on parameter sets that lacked comprehensive calibration of dynamic material properties, including HEL values in the JH-2 model. To address these issues, recent studies have refined the JH-2 model parameters to more accurately represent the behaviour of float glass under high strain-rate conditions. Zhang et al. [11] and Zhou et al. [12] introduced systematic modifications to tensile strength, pressure coefficients, and HEL values, offering a more realistic framework for simulating brittle failure in LG systems. However, these refinements have not yet been universally adopted or applied in studies involving large rigid body impacts.

In light of these limitations, the present study undertakes a methodical calibration of JH-2 material model coefficients, based on a meta-analysis of previous refinements. It further incorporates realistic dynamic material properties for both float glass and PVB interlayers and integrates boundary components such as silicone sealants into the FE framework. Section 3 of this thesis details the development and validation of a robust FE model for simulating wood block impacts on LG, including a thorough mesh sensitivity analysis. Section 4 introduces the development of perforation vulnerability curves for LG systems with varying interlayer thicknesses and projectile configurations. By expanding the scope of current modelling approaches and addressing previously overlooked variables, this aims to enhance the predictive accuracy of impact simulations and contribute to the evolution of performance-based design and safety evaluation for LG systems exposed to extreme impact conditions.

CHAPTER 3

METHODOLOGY

3.1 Introduction to the Research Process

This chapter presents the research methodology through a detailed description on the FE based procedure used in this study. The study simulates laboratory impact tests from prior research [3], [11] to validate a robust FE model for predicting the dynamic behaviour of LG panels under impact loading. Section 3.2 details the FE model, which represents a 7.88 mm thick LG panel and a wood impactor. Section 3.3 elaborates on the material models, with the Johnson-Holmquist Ceramics (JH-2) model capturing the brittle fracture of float glass, the piecewise linear plasticity model addressing PVB's elastoplastic behaviour, and the rigid body model representing the wood impactor. Section 3.4 presents a mesh convergence study evaluating various mesh configurations, identifying a 5 mm in-plane mesh with (2/2/2) through-thickness discretization as optimal for balancing accuracy and computational efficiency (refer Section 3.4 for notations). Section 3.5 validates the FE model against the experimental data, comparing deflection, strains, and fracture patterns, using statistical metrics (RMSE, R^2, MAPE) confirming the model's accuracy. This research provides a validated FE framework for advancing the understanding and design of LG panels under impact conditions, which is the aim of this study.

3.2 Finite Element Model

Finite element (FE) simulations are widely employed to model impact scenarios, providing a dependable way to validate and forecast results. This technique is especially beneficial in situations where conducting experiments is overly costly and demands substantial resources and effort to carry out. In this study, the LS-DYNA explicit FE software was employed to simulate the laboratory test depicted in Fig. 3.1, which was carried out by earlier researchers [3], [11]. Fig. 3.2 showcases the FE model, which was developed for the LG plate and the rigid body impactor. According to the experimental setup [3], the model consists of a 7.88 mm thick LG panel comprising a 3 mm front glass, a 1.88 mm interlayer, and a 3 mm back glass. The total dimensions of the panel are 2000 mm × 1200 mm. Due to symmetry, only one-quarter of the model was used in the numerical simulation. As shown in Fig. 3.2, two edges of the plate are simply supported (refer to Section 4.2 for details on the support conditions), while the remaining two edges exhibit symmetrical boundaries.

The FE model utilized three-dimensional (3D) solid elements to accurately represent the glass panels, interlayer, and the impactor. For both the glass and interlayer, an in-plane mesh of dimensions 5 mm × 5 mm was implemented and comprised of two elements through the thickness. This configuration was chosen to guarantee precise depiction of both stress and deformation parameters, as illustrated in Fig. 3.2.

Comprehensive mesh sensitivity analyses, which are delineated in more detail in Section 3.4, validated this mesh configuration. The impactor, constructed from wood with a mass of 4 kg and a contact surface measuring 100 mm × 50 mm, was launched at a velocity of 15 m/s directly towards the centre of the LG system under conditions comparable to those observed in experimental setups. To enhance the fidelity of contact interactions and simulation precision, the contact surface of the impactor was meshed to correspond with the mesh size of the glass panel. The LG system was simulated by merging duplicate nodes at the interfaces of the three layers, which effectively modelled the glass as a fully bonded assembly. This practice ensured seamless continuity amongst the layers, facilitating direct force transfer across the interfaces. Although each individual layer preserved its unique material characteristics, the continuous interfaces facilitated an accurate simulation of interlayer interactions and the distribution of loads.

The finite element (FE) model incorporated material model 110 (MAT_JOHNSON_HOLMQUIST_CERAMICS/ JH-2) specifically for float glass to effectively simulate its brittle fracture properties. Concurrently, material model 24 (MAT_PIECEWISE_LINEAR_PLASTICITY) was employed for the polyvinyl butyral (PVB) interlayer in order to accurately depict its elastoplastic characteristics. For the rigid wood block impactor, material model 20 (MAT_RIGID) was utilized, ensuring a rigid body representation. This selection of material models was deliberate, aiming to accurately replicate the unique mechanical responses of each constituent as elaborated in Section 3.3. In modelling the interaction between the wood block and the LG, an AUTOMATIC_SURFACE_TO_SURFACE contact algorithm within LS-DYNA was applied. This involved activating the SOFT constraint option to facilitate precise transmission of forces and maintain realistic contact behaviour throughout impact occurrences.

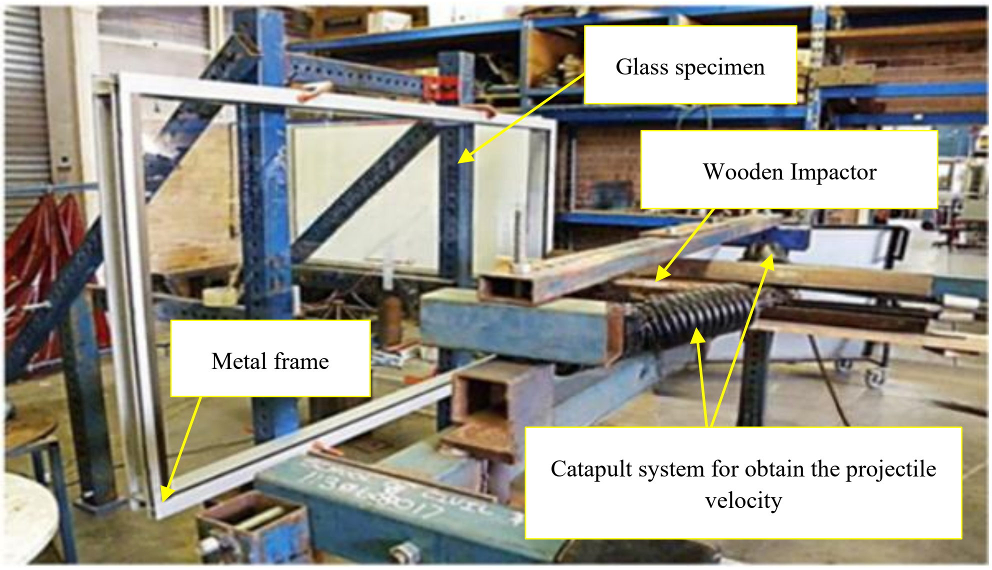

Fig. 3.1: Experimental setup for the impact test

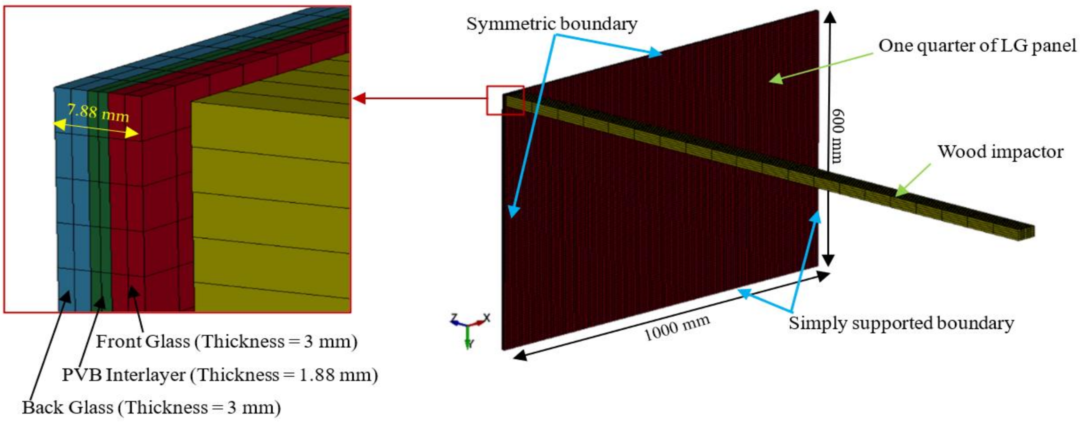

Fig. 3.2: Developed FE model for the impact test

3.3 Material Models used in LS-DYNA

3.3.1 Float Glass

This research employs the material model 110, commonly known as JH-2, to analyse how float glass behaves when subjected to impact forces. Glass typically experiences brittle failure, with its failure strength significantly influenced by the strain rate as evidenced in prior studies [2], [10]. Utilizing static linear elastic material models can lead to substantial underestimations of the material's performance, particularly during impact scenarios characterised by high strain rates. Numerous experimental studies have been conducted to explore the dynamic behaviour of float glass. Theoretical calculations by Brown [67] suggested that the dynamic strength of glass might be as much as triple its static strength, a hypothesis supported by experimental findings. Holmquist et al. [65] conducted dynamic assessments of float glass using a Split Hopkinson Pressure Bar (SHPB) test and formulated a detailed dynamic material model for glass, which underpins the JH-2 material model within LS-DYNA. Similarly, Peroni et al. [68] examined the impact of dynamic strain rates on the compressive and tensile strengths of glass through SHPB testing, revealing insights into its behaviour across numerous pressure domains. Bourne et al. [69] performed plate impact experiments on a variety of composite glasses to investigate the phenomenon of failure waves in glass subjected to shock. Subsequently, Feng [70] introduced a theoretical framework to explain the formation and propagation of failure waves within glass.

In the early 1990s, Johnson and Holmquist [64], [65] proposed the advanced JH-2 constitutive model for brittle materials like ceramics, focusing on their mechanical response and failure under high strain rates and pressures typical of ballistic impacts. The JH-2 model has since been extensively adopted for simulating impact and blast loads on thin glass panels [2], [3], [11], [12], [23], [31], [66], [71]. Over the years, various researchers have modified the parameters of the JH-2 model to consider the composition of modern glass, which often has a reduced SiO_2 content in comparison to older glass types. Hidallana-Gamage et al. [66] introduced modifications to the JH-

2 model by lowering the tensile strength, leaving other parameters unaltered. This approach was further refined by Zhang et al. [11], who not only reduced the tensile strength more significantly but also made adjustments to additional parameters. These adjustments included the lowering of pressure coefficients, the Hugoniot Elastic Limit (HEL), and the pressure component associated with the HEL. Moreover, Zhang et al. [11] lowered the values for the intact normalised strength parameters A and N while increasing the C strength parameter. Zhou et al. [12], in their study, maintained the tensile strength figures established by Zhang et al. [11], yet opted for a more substantial reduction in pressure coefficients as well as in the intact normalised strength parameter A. The values for HEL and its associated pressure component, as determined by Zhou et al. [12], were set in an intermediate range between the results of Holmquist et al. [65] and Zhang et al. [11], but with a preference towards those determined by Holmquist et al. [65]. The variations observed in the results can be ascribed to the different methodologies employed for evaluating the HEL. In the study by Zhang et al. [11], a pseudo HEL was introduced, which was calculated by utilizing both the peak uniaxial strength and the corresponding pressure values obtained from the SHPB tests. Conversely, Holmquist et al. [65] employed plate impact tests, recognized as the conventional and more precise method for the assessment of HEL values. Accordingly, the HEL parameters reported by Zhou et al. [12], which closely align with these plate impact-based values, were adopted in this study. Taking into account these methodological discrepancies, the current investigation utilizes the JH-2 model parameters, which are comprehensively detailed in Table 3.1, to accurately simulate the behaviour of float glass.

Table 3.1: Material parameters used for JH-2 model [11], [12]

Parameters	**Value**
Density (RO)	2530 kg/m^3
Shear modulus (G)	26.9 GPa
A	0.75
B	0.2
C	0.035
M	1.0
N	0.72
Reference strain (EPSI)	1.0
Maximum Tensile Pressure (T)	27.8 MPa
Maximum Normalised Fracture Strength (SFMAX)	0.5

HEL	4.5 GPa
HEL pressure (PHEL)	2.4 GPa
Bulk (β/BETA)	1.0
D1	0.043
D2	0.85
K1	43.2 GPa
K2	-67.2 GPa
K3	153.2 GPa

The JH-2 framework integrates models for strength, damage, and strain rate effects along with an equation of state (EOS). The normalized material strength, denoted as (σ^*), is formulated (refer to Equation 1) using normalized intact strength (σ_i^*), normalized fractured strength (σ_f^*), and the damage scalar D.

$$\sigma^* = \sigma_i^* - D(\sigma_i^* - \sigma_f^*) \tag{1}$$

Stresses are normalized by dividing the real stress (σ) by the equivalent stress (σ^{HEL}) at the Hugoniot Elastic Limit (HEL):

$$\sigma^* = \frac{\sigma}{\sigma^{HEL}} \tag{2}$$

Equations 3 and 4 define the normalized intact and fractured stresses, accounting for strain rate influences. Parameters A, B, C, and M describe material strength, whereas P^* and T^* signify normalized pressure and peak tensile hydrostatic pressure. The normalized strain rate, $\acute{\varepsilon}^*$ is derived by dividing the strain rate by the reference rate of 1.0 s^{-1} [71], [72].

$$\sigma_i^* = A(P^* + T^*)^N(1 + C \ln \acute{\varepsilon}^*) \tag{3}$$

$$\sigma_f^* = B(P^*)^M(1 + C \ln \acute{\varepsilon}^*) \tag{4}$$

Fracture damage accumulation (D) is given by:

$$D = \sum \frac{\Delta\varepsilon_p}{\varepsilon_p^f} \tag{5}$$

where $\Delta\varepsilon_p$ represents the increment in plastic strain per integration cycle, and ε_p^f denotes the fracture strain under uniform pressure P

$$\varepsilon_p^f = D_1(P^* + T^*)^{D_2} \tag{6}$$

where D_1 and D_2 are material-specific constants concerning fracture damage.

Equation 7 describes the hydrostatic pressure in the intact material, characterized by constants K_1, K_2, and K_3.

$$P = K_1\mu + K_2\mu^2 + K_3\mu^3 + \Delta P \tag{7}$$

where $\mu = \frac{\rho}{\rho_0} - 1$, with ρ as the current density and ρ_0 denoting the initial density.

3.3.2 PVB Interlayer

Extensive prior research has established that the mechanical characteristics of polyvinyl butyral (PVB) exhibit a pronounced dependency on the strain rate [3], [4], [73], [74], [75]. In scenarios characterized by gradual loading, PVB primarily displays viscoelastic behaviour. In contrast, when subjected to rapid tensile loads, its response shifts to exhibit elastoplastic characteristics and can even demonstrate brittleness. This necessitates the incorporation of an elastoplastic material model in numerical simulations. To fulfil this requirement, the material model 24 available in LS-DYNA, identified as MAT_PIECEWISE_LINEAR_PLASTICITY, is adopted for modelling the PVB interlayer within the current FE model framework. The reliability and accuracy of this material model have been substantiated by previous investigations [66], [73]. Table 3.2 delineates the material properties of PVB that are utilised within the present FE model.

Table 3.2: Material properties of PVB interlayer

Parameters	**Value**
Density (RO)	1100 kg/m^3
Young's modulus (E)	221 MPa
Poisson's Ratio	0.485
Yield stress	11.41 MPa
Tangent modulus	5.25 MPa
Failure stress	28 MPa
Failure strain	2

The relationship between stress and strain, as illustrated in Fig. 3.3, encompasses a detailed depiction of the mechanical response, particularly highlighting the yield stress, failure stress, and the strain at failure.

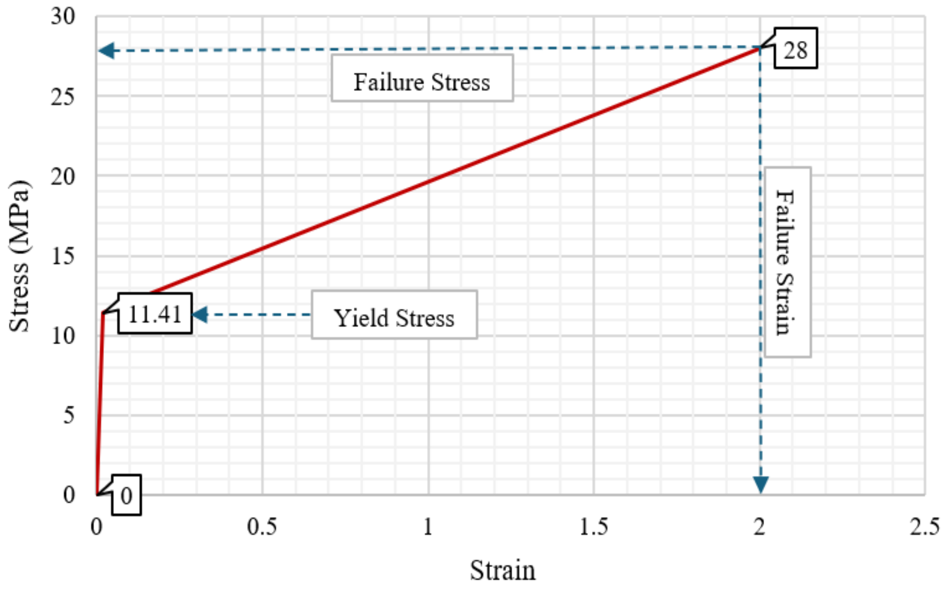

Fig. 3.3: Stress-strain variation of the PVB [22]

3.3.3 Wooden Projectile

The wooden projectile, as delineated in the experimental design outlined in reference [3], was modelled using 3D solid elements. This projectile features a contact surface with dimensions of 100 mm by 50 mm and an overall length of 1.6 m. According to the specifications given in experiment [3], the impactor employed in this setup is constructed from hard pine. As a result of these material properties and design considerations, the experiment revealed no notable permanent deformation occurring in the impactor during the impact event. Consequently, the wooden impactor has been treated as a rigid body in the numerical modelling process, utilising material model 20, known as MAT_RIGID, to reflect its inherent rigidity accurately. For a comprehensive understanding of the impactor's characteristics, detailed parameters are provided in Table 3.3.

Table 3.3: Parameters used for the wooden impactor

Parameters	**Value**
Mass	4 kg
Density (RO)	500 kg/m^3
Young's modulus (E)	9 GPa
Length	1.6 m

3.4 Mesh Convergence Study

An extensive mesh sensitivity analysis was conducted to evaluate the numerical accuracy of the currently developed FE model. This comprehensive analysis focused on two pivotal response parameters: the time-dependent deflection profiles at the central region of the glass panel and the total internal energy-time histories across the entire LG panel. A series of simulations was executed with nine varied mesh configurations: specifically, 100 × 60 × 6, 200 × 120 × 6, 250 × 150 × 6, 400 × 240 × 6, 500 × 300 × 6, 200 × 120 × 3, 200 × 120 × 5, 200 × 120 × 7, and 200 × 120 × 8. For instance, a mesh setup identified as 100 × 60 × 6 indicates 100 elements distributed along the panel's length (x-direction), 60 elements arrayed along its width (y-direction), and a division of 6 elements across the thickness (z-direction) of the panel. Similarly, the specifications for the remaining configurations stipulate the number of elements across these three dimensions. Variations in the thickness-wise element count were achieved by segmenting the two glass layers and the interlayer film into more refined mesh units spanning the thickness, as depicted in Fig. 3.2. For example, the setting featuring three elements through the thickness is equivalent to having one element per individual layer. Conversely, the arrangement with five elements through the thickness incorporates two elements per glass ply and a single element for the interlayer film. These arrangements are denoted as (1/1/1) and (2/1/2), respectively, in this investigation. Furthermore, notations such as (2/2/2), (3/1/3), and (3/2/3) represent the through-thickness mesh configurations for six, seven, and eight elements, respectively, within the thickness of the LG plate.

Fig. 3.4 and Fig. 3.5 illustrate the results from the mesh sensitivity analysis concerning the central deflection corresponding to different mesh size arrangements. Specifically, Fig. 3.4 displays comparisons among various in-plane mesh sizes, which include measurements of 2 mm, 2.5 mm, 4 mm, 5 mm, and 10 mm. Conversely, Fig. 3.5 focuses on changes in through-thickness elements while maintaining an in-plane mesh size of 5 mm. The trend that emerges is that finer meshes lead to increased deflections, particularly noticeable after 10 ms, where the coarser mesh arrangements, such as 100 × 60 × 6, struggle to provide accurate estimates of central deflection. In contrast, more refined mesh configurations like 200 × 120 × 6, 250 × 150 × 6, 400 × 240 × 6, and 500 × 300 × 6 demonstrate a convergence towards numerical accuracy, with deflection settling around 120 mm at 18 ms, compared to approximately 104 mm observed for the coarsest mesh at 100 × 60 × 6. Beyond the configuration of 200 × 120 × 6, the improvements in accuracy lessen, suggesting diminishing returns from further mesh refinement. Nevertheless, the computational time escalates exponentially with increased resolution. Notably, completing the simulation with the 500 × 300 × 6 configuration demanded more than 21 hours and 39 minutes on an 11th Gen Intel Core i5-11400H processor (6 cores, 12 threads, 2.7 GHz base, 4.5 GHz max boost) when conducted independently. When executing multiple simulations concurrently, the total simulation time may extend over several days, underlining the impracticality of performing a vast number of simulations. Through-thickness elements (see Fig. 3.5) play a crucial role in accurately modelling LG panels, highlighting the importance of mesh refinement. Coarse models, such as (1/1/1) with a single element per layer, failed to adequately represent interfacial behaviour and nonlinear responses. In contrast, finer discretisation like (2/2/2), (3/1/3), and (3/2/3) showed improved accuracy and stability in predicting deflections. However, finer meshes increased simulation time, and the accuracy differences among (2/2/2), (3/1/3), and (3/2/3) were slight, indicating that (2/2/2) offers an effective compromise between accuracy and computational cost.

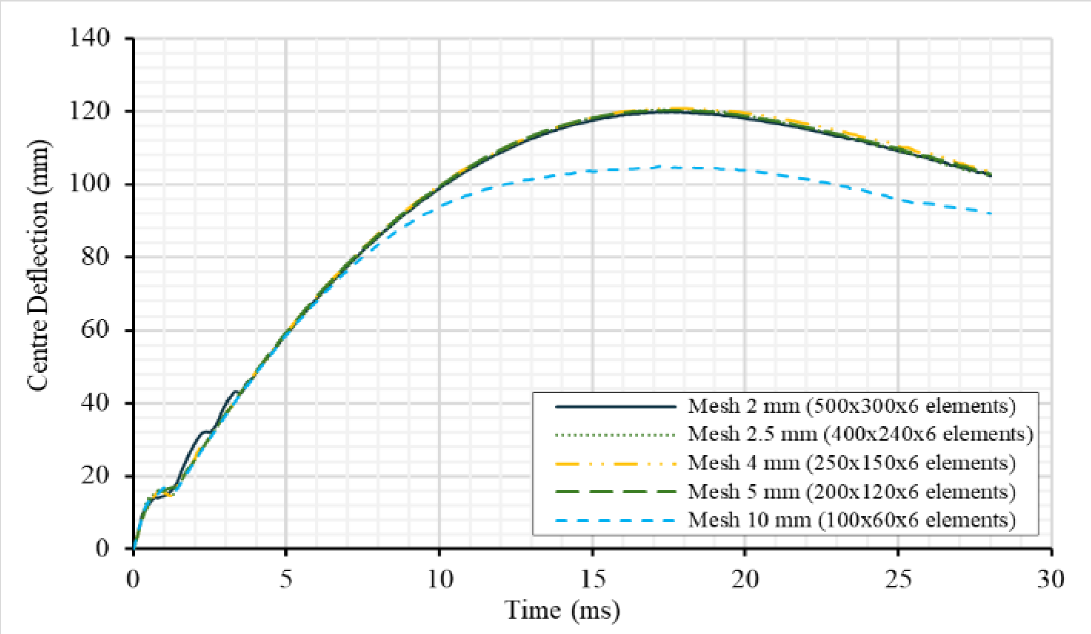

Fig. 3.4: Deflection-time histories of LG panel (Different in-plane mesh sizes)

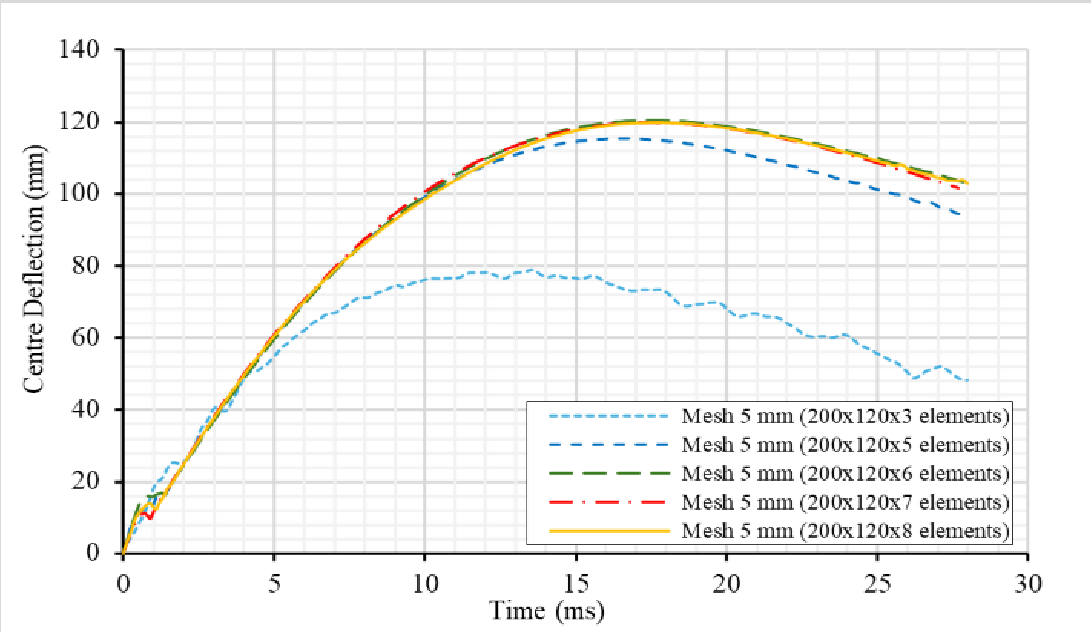

Fig. 3.5: Deflection-time histories of LG panel (Different through-thickness elements)

Fig. 3.6 and Fig. 3.7 present a comparative analysis of the total internal energy of the LG panel model, reduced to a quarter model for simulation purposes, with different in-plane mesh sizes (as depicted in Fig. 3.6) and distinct through-thickness element arrangements (as depicted in Fig. 3.7). The temporal evolution of the total internal energy showed patterns closely resembling those identified in deflection studies. It was observed that larger in-plane mesh sizes lacked precision in capturing the transient energy shifts that arise during impact loading and subsequent rebound phases. Conversely, more detailed in-plane mesh configurations, such as 200 × 120 × 6, 250 × 150 × 6, 400 × 240 × 6, and 500 × 300 × 6, improved the detail level of these energy variations, facilitating a more precise approximation towards energy convergence. The selection of through-thickness configurations greatly influenced the time-dependent internal energy profiles, especially during the load application phase. Coarser through-thickness configurations, exemplified by (1/1/1), resulted in discrepancies in the peak energy readings and failed to identify intricate energy dissipation mechanisms. On the other hand, finer configurations, including options like (2/2/2), (3/1/3), and (3/2/3), consistently demonstrated stable and convergent energy trends, with marginal advantages observed for the latter configurations. Given the computational demands associated with the (3/1/3) and (3/2/3) setups, the (2/2/2) configuration emerges as the most pragmatic choice for efficient computational application.

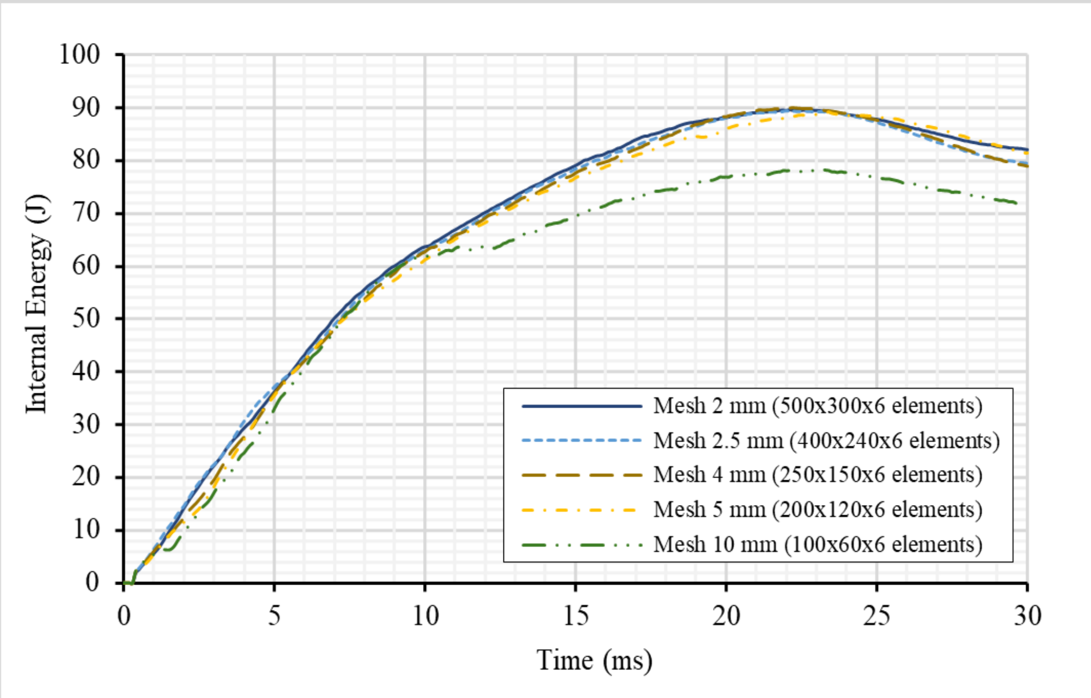

Fig. 3.6: Total internal energy variations of LG panel (Different in-plane mesh sizes)

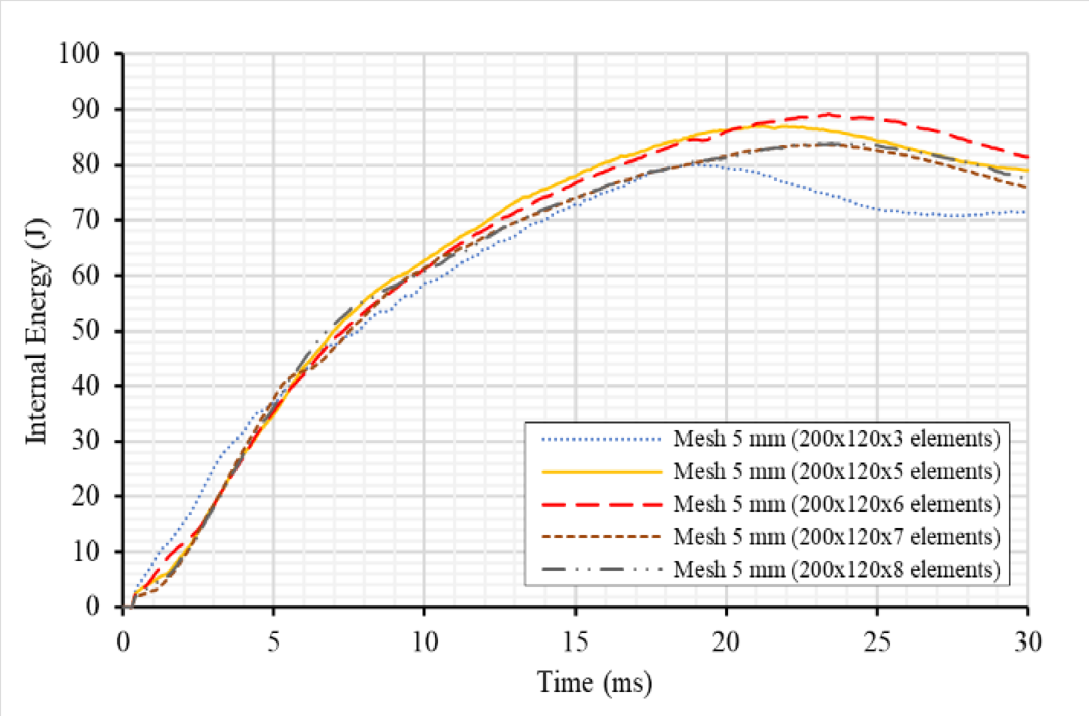

Fig. 3.7: Total internal energy variations of LG panel (Different through-thickness elements)

The data illustrated in Figs. 3.4–3.7 highlight the fundamental compromise that exists between achieving numerical precision and ensuring computational efficiency. While employing the most refined in-plane mesh configurations and comprehensive through-thickness setups leads to maximal accuracy, it also substantially elevates the computational expense, thereby making it impractical for extensive explorative studies. An optimal configuration has been identified, which employs a 5 mm in-plane mesh in conjunction with a (2/2/2) through-thickness discretization. This particular setup manages to achieve a high degree of accuracy, all the while considerably minimizing the required computational time. This configuration proves especially advantageous for conducting numerous FE simulations and exploring parametric studies, where computational efficiency is critically important. Therefore, this configuration will be used for subsequent analyses detailed in the remainder of this study.

3.5 Validation of the FE model

To guarantee the accuracy of numerical simulations, every essential condition specified in experiments [3], [11] has been integrated, following ASTM standards [9]. The FE analysis results for central deflection, LG panel fracture, as well as stress and strain of various components, were contrasted with the existing experimental data, detailed below.

3.5.1 Maximum centre deflection and Deflection time history curves

In the conducted experiment, the deflection occurring at the midpoint of LG was recorded utilising a high-speed camera, as discussed in reference [11]. Following this, the recorded data underwent processing through a tracking algorithm to derive the deflection time history, which is displayed as an experimental curve in Fig. 3.8. Furthermore, Fig. 3.8 illustrates centre deflection time histories as predicted by the FE model established in the current study. Additionally, for comparative analysis, deflection time histories obtained by previous researchers, including Zhang et al. [11] and Holmquist et al. [65], are also depicted in Fig. 3.8 to substantiate the accuracy and validity of the present FE model. It is noteworthy that the study by Holmquist et al. [65] did not distinctly exhibit deflection time histories; however, their model parameters were incorporated within the FE model utilised by Zhang et al. [11], thereby enriching the numerical framework of the current research.

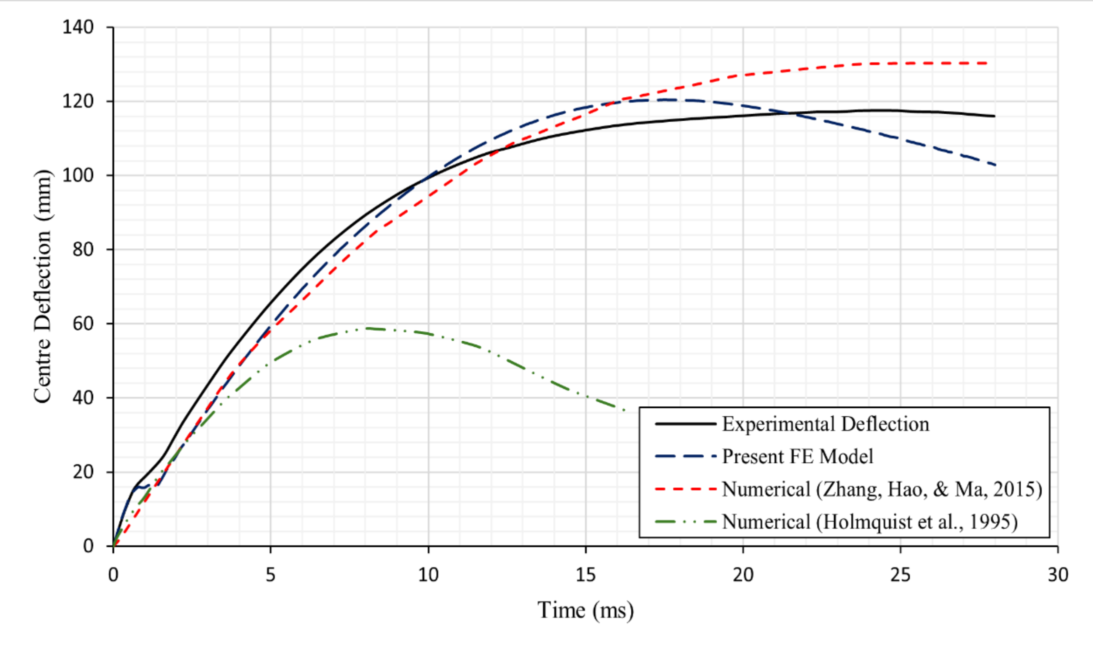

Fig. 3.8: Comparison of centre deflection time histories of LG panel

Fig. 3.8 provides a comparative analysis of the centre deflection time histories derived from experimental findings, the current FE model, and the computational models developed by Zhang et al. [11] and Holmquist et al. [65]. Experimentally, the maximum centre deflection is observed to be approximately 118 mm. The FE model from the current study predicts a peak deflection near 120 mm, showcasing a remarkable correlation with the experimental measurements, covering both the peak deflection and the entire deflection profile over time. Conversely, the simulation employing the material properties proposed by Holmquist et al. [65] dramatically underestimates the deflection, yielding a maximum value of only 58 mm. This notable discrepancy is primarily due to the overestimation of glass material strength parameters in the Holmquist et al. [65] model, which is related to the SiO_2 content in older float glass. Older glass varieties with a higher SiO_2 concentration displayed superior tensile and compressive strength, in contrast to more recent glass compositions with reduced SiO_2 levels [22]. Meanwhile, the model by Zhang et al. [11] forecasts a maximum deflection of 132 mm, surpassing the experimental outcome and diverging more drastically in the comprehensive deflection time profile. The present FE model not only predicts the maximum deflection with enhanced accuracy but also more accurately mirrors the overall deflection time history observed experimentally when compared to the FE model from Zhang et al. [11]. This conclusion is further corroborated by the statistical evaluation presented in Table 3.4, where statistical measures such as root mean square error (RMSE), coefficient of determination (R^2), and mean absolute percentage error (MAPE) substantiate that the current FE model demonstrates superior alignment with the experimental results.

Table 3.4: Statistical evaluation of the FE model results

Model	RMSE	R^2	MAPE
Present FE Model	5.582229	0.967208	6.367891
Numerical (Zhang et al. 2015)	8.650542	0.921253	10.50168

Moreover, a high-speed camera capable of recording 8000 to 10000 frames per second (fps) was employed to ascertain the deflection metrics at intervals of 0.1 ms throughout the experimental procedures, as referenced [3]. Upon examining the magnified segment of Fig. 3.8, it is evident that the FE model devised by Zhang et al. [11] inadequately represents the immediate post-impact response of LG. Conversely, the FE model developed in this study replicates the experimental outcomes, especially during the initial impact phase.

3.5.2 Maximum strains

In order to enhance the validation of the numerical model's accuracy, an extensive calibration process has been implemented focusing on three specific LG samples, designated as Spec. No. 1, 2, and 3, which were previously analysed through empirical laboratory investigations by Zhang et al. [3]. The observed maximum strain values occurring in the rear glass layer, as derived from the laboratory experiments, have been systematically evaluated in comparison with the outcomes of the current numerical model, as well as juxtaposed with the findings derived from Zhang's FE model. These comparative analyses are comprehensively presented within Table 3.5.

Table 3.5: Comparison of experimental strains and numerical strains

Spec. No.	Dimension (mm)	Thickness (mm)		Impact speed (m/s)	Maximum Glass Strain		
		Glass	PVB		Experimental	Numerical (Zhang et al. (2013))	Numerical (Present FE model)
1	2000 × 1100	3	1.52	15	0.00154	0.00152	0.001571
2	2000 × 1100	3	1.88	15	0.00107	0.00101	0.001056
3	2000 × 1100	6	1.52	15	0.00089	0.00094	0.000887

Table 3.5 illustrates that the current FE model has a higher error for specimen 1 (2%) compared to Zhang et al. [3] (1.3%), but reduced errors for specimens 2 and 3, with specimen 2 decreasing from 5.61% to 1.3% and specimen 3 from 5.62% to 0.34%. These differences arise from numerical inaccuracies, inherent assumptions in material models, and idealised boundary conditions. Nonetheless, the present FE model provides accurate lab test predictions, surpassing the FE model by Zhang et al. [3], [11] in most scenarios.

3.5.3 Fracture and stress analysis of LG

In order to examine the patterns of fractures and the propagation of stress waves, analyses were conducted on specimens 1, 2, and the specific specimen outlined in Section 3.5.1. Fig. 3.9 and Fig. 3.10 provides a representation of the initiation and progression of fractures in the glass layers at the front and back of the LG, accompanied by the respective stress variations observed at various time intervals (note that only a quarter of the model is illustrated here). The inclusion of the glass specimen detailed in Section 3.5.1 was intentional to offer an in-depth comparison of how fractures develop, and stress distributes over time. This examination employs an erosion technique within the FE method framework to simulate the onset and spread of cracks. As depicted in Fig. 3.9, the front ply of the glass demonstrates a complex network of radial and circumferential fractures radiating from the point of impact, expanding in a circular manner in response to the propagating stress wave. The fractures that are furthest from the origin begin at the lower boundary, which is likely due to localized stress concentration. In contrast, the rear glass ply exhibits a delayed fracture initiation, mainly comprising radial fracture patterns (refer to Fig. 3.10). This delay can be ascribed to the front glass's exposure to direct impact forces, leading to a concentric fracture pattern. In contrast, the rear glass experiences failure predominantly from bending tensile stresses induced by the impact, resulting in radial cracks akin to the yield failure observed in concrete panels. Glass components will suffer sudden failure without any forewarning when the stress intensity at a crack tip in tension surpasses a critical threshold.

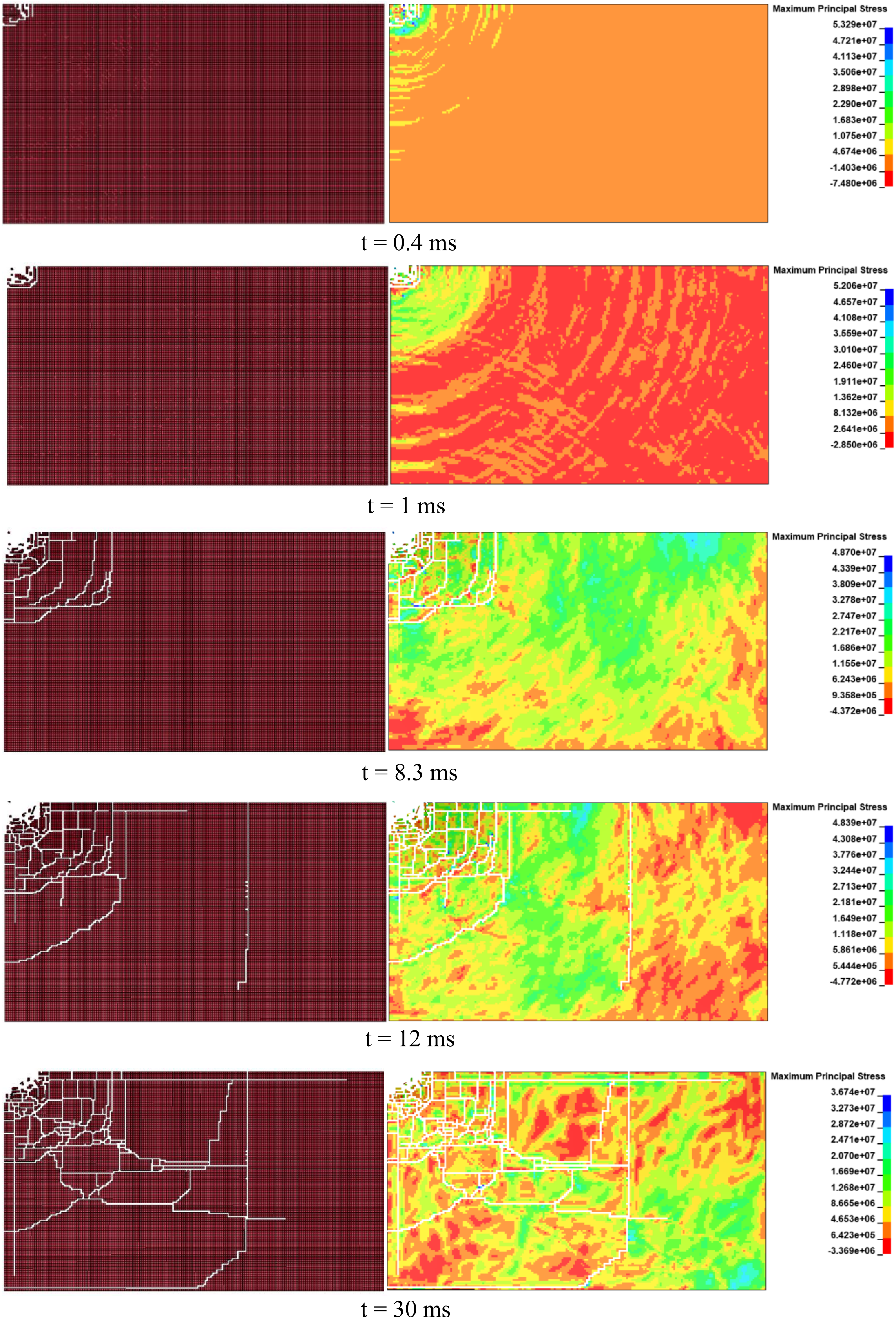

(a) Crack Propagation (b) Stress Variation

Fig. 3.9: Fracture patterns and stress variations of Front glass ply of LG system

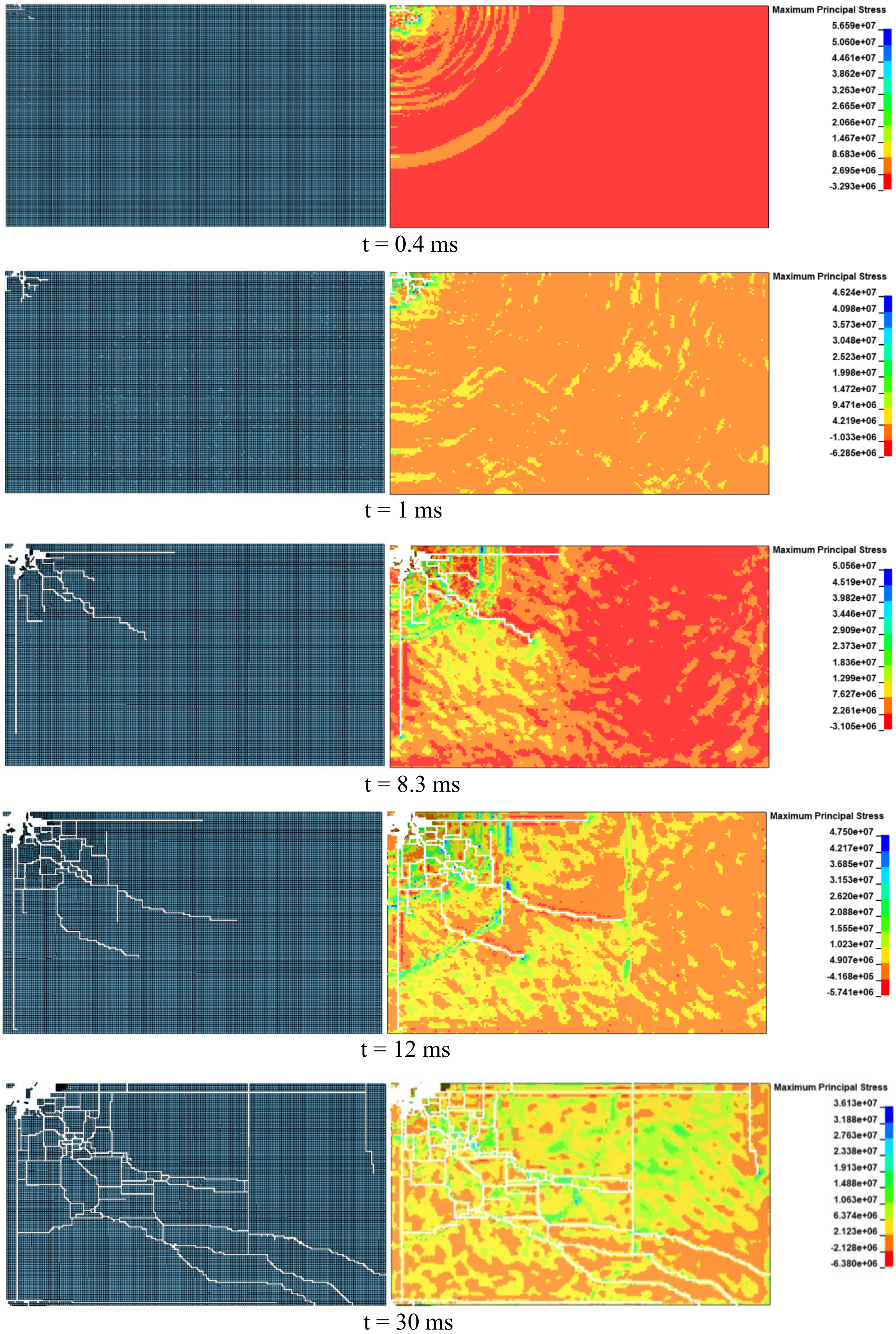

(a) Crack Propagation (b) Stress Variation

Fig. 3.10: Fracture patterns and stress variations of Back glass ply of LG system

Fig. 3.11 offers an in-depth comparative study of the fracture patterns as observed in test specimens 1 and 2 when juxtaposed with the fracture patterns anticipated by the FE models developed in the present research. To further enrich this comparative evaluation, we have integrated the cracking patterns derived from the FE model by Zhang et al. [3]. This inclusion underscores both the disparities and correspondences in crack propagation and distribution, facilitating a nuanced understanding of the correlation between empirical observations and numerical predictions generated through FE models.

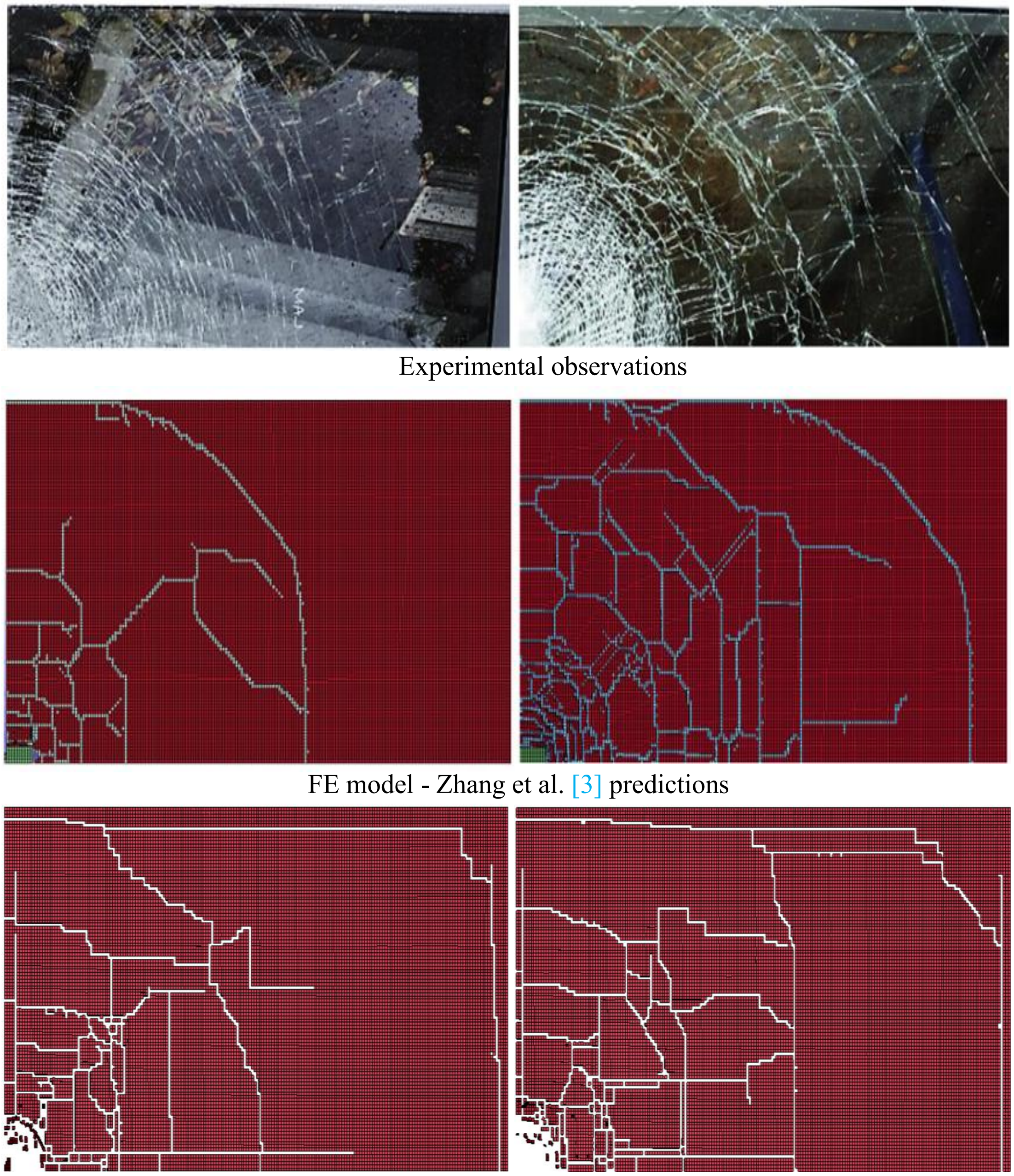

(a) Fracture pattern of Specimen 1 (b) Fracture pattern of Specimen 2

Fig. 3.11: Comparison of fracture patterns of LG panel

As depicted in Fig. 3.11, the crack propagation paths within the present FE model manifest in almost the same regions in both analysed specimens, closely aligning with the experimental observations. However, it is noteworthy that the crack dimensions predicted by both FE simulations exceed those seen in experimental data. While both numerical models demonstrate similar patterns in crack initiation, there is a marked difference in terms of crack density and the characteristics of secondary fracture developments. These discrepancies can be attributed to inherent material and numerical modelling limitations. Real glass is not perfectly homogeneous; microscopic flaws, residual stresses from manufacturing, surface damage, and edge defects strongly influence crack initiation and propagation. In contrast, the FE model assumes glass to be homogeneous and isotropic, which cannot capture the true flaw distribution governing experimental fracture paths. In addition, crack propagation in FE simulations is strongly influenced by mesh size and orientation. Even with mesh refinement, cracks tend to follow element boundaries or preferred numerical directions, whereas experimental cracks evolve in response to stress wave interactions and pre-existing flaw networks. These factors collectively contribute to the observed differences in crack density and fracture patterns between experimental and numerical results.

Through an in-depth assessment of the comparative outcomes between the FE model and laboratory experiments, which concentrated on various parameters such as maximum deflection, temporal evolution of central deflection, peak strain values, fracture mechanisms, and stress propagation trajectories, it becomes evident that the numerical model developed in the current study offers a precise simulation of the impact reactions exhibited by LG panels subjected to testing under conditions emulating rigid body impacts. As a result of these findings, the modelling technique developed in the current study has been adopted for subsequent studies to thoroughly investigate and evaluate the impact performance of LG.

CHAPTER 4

RESULTS AND DISCUSSIONS

4.1 Introduction

This chapter presents a detailed investigation into the results derived from numerical simulations, concentrating on crucial response parameters that are difficult to quantify experimentally. These parameters include the attributes of energy absorption and the distribution of stress across varying components, which are vital for both design and analysis. Due to the significant costs and resources involved in setting up experimental facilities for different impact scenarios, FE analysis was employed strategically to simulate over 276 distinct impact scenarios. The outcomes include the formation of perforation vulnerability curves, which deliver a systemic framework for understanding the perforation performance of LG when impacted by wooden projectiles. This methodological approach delivers insights that extend beyond the confines of traditional laboratory experiments, offering a more comprehensive understanding of the phenomena under study.

4.2 Effects of Silicone Sealant, Aluminium Frame and PVB Interlayer

According to AS1288: 2021 [76], a frame is characterized as a construct engineered to provide support to the entire length of a glazed panel's edge. It is generally composed of robust materials such as timber, metal, or composite configurations that include elements like glass and silicone sealants. Notably, silicone sealant can function beyond simply offering protection against weather conditions; it also plays a crucial role in structurally transmitting loads from the glass panel to the surrounding support system. In contrast to this, Zhang's FE model [3], [11] did not incorporate the presence of silicone sealant. The numerical analysis in Zhang's model assumed a direct interaction between the glass pane and its aluminium frame, effectively ignoring the thin silicone sealant layer used in experimental conditions. Consequently, this oversight led to an unnatural accumulation of stress along the edges of the glass. In this study, however, the silicone sealant is explicitly modelled, as depicted in Fig. 4.1, and its impact is assessed through the comparison of deflection time histories. The frame specifications are tailored to align with the parameters of the experimental design, which specifies an aluminium frame with a width of 15 mm and a thickness of 6 mm. Detailed material properties for both the aluminium and silicone sealant are systematically presented in Table 4.1. In accordance with ASTM standards [77], [78], the silicone sealant's bite measurement is set at 15 mm, and its thickness at 6 mm.

Table 4.1: Material parameters of Aluminium frame and silicone sealant used in the FE model

Material Parameters	Aluminium Frame	Silicone Sealant
Density (RO)	2700 kg/m^3	1100 kg/m^3
Young's modulus (E)	70 GPa	2.3 MPa
Poisson's Ratio	0.3	0.495
Yield stress	-	2.3 MPa

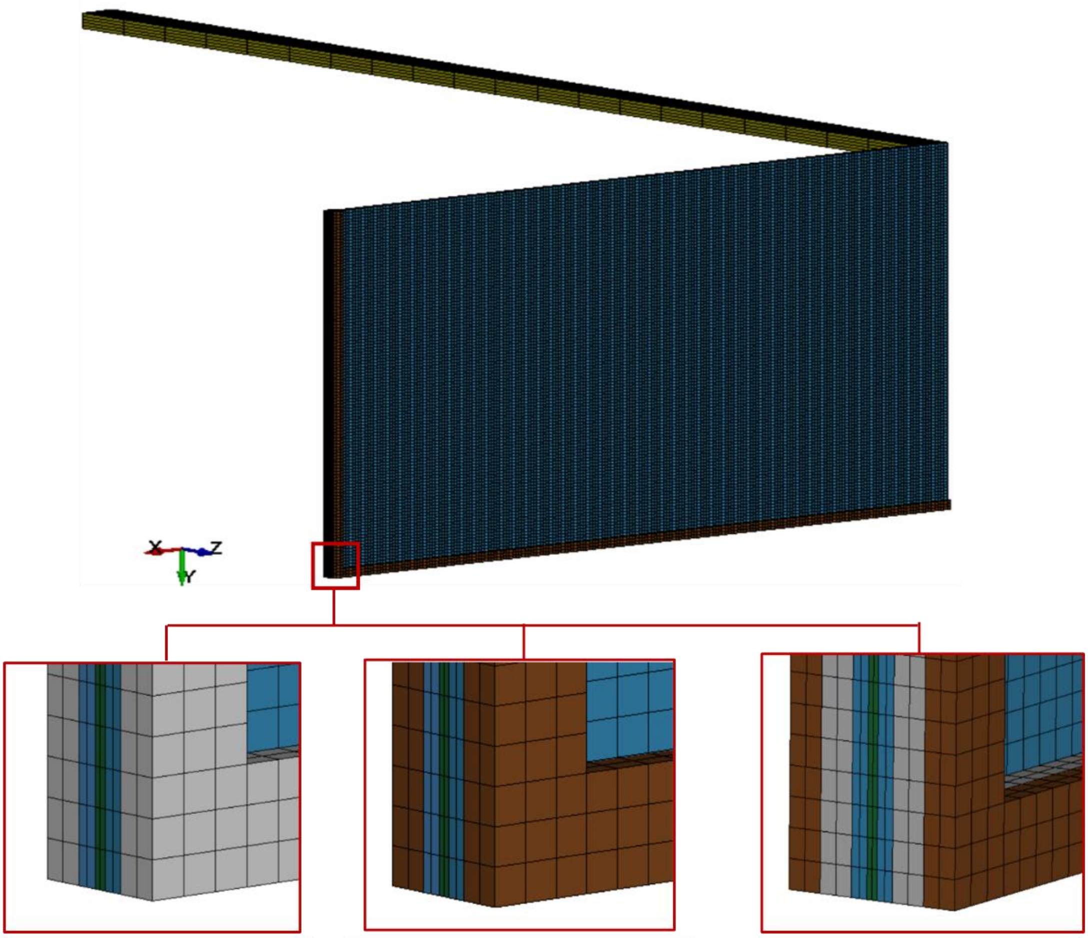

(a) Only silicone sealant (SS) (b) Only aluminium frame (AF) (c) Both AF & SS

Fig. 4.1: FE model with different boundary conditions

This study examines four boundary conditions: a simply supported edge (see Section 3), a silicone sealant edge, an aluminium frame edge, and a hybrid setup with both silicone and a metal frame. Fig. 4.2 illustrates the deflection time histories for LG panels, highlighting the crucial role of silicone sealants in mitigating stress concentrations and improving structural integrity.

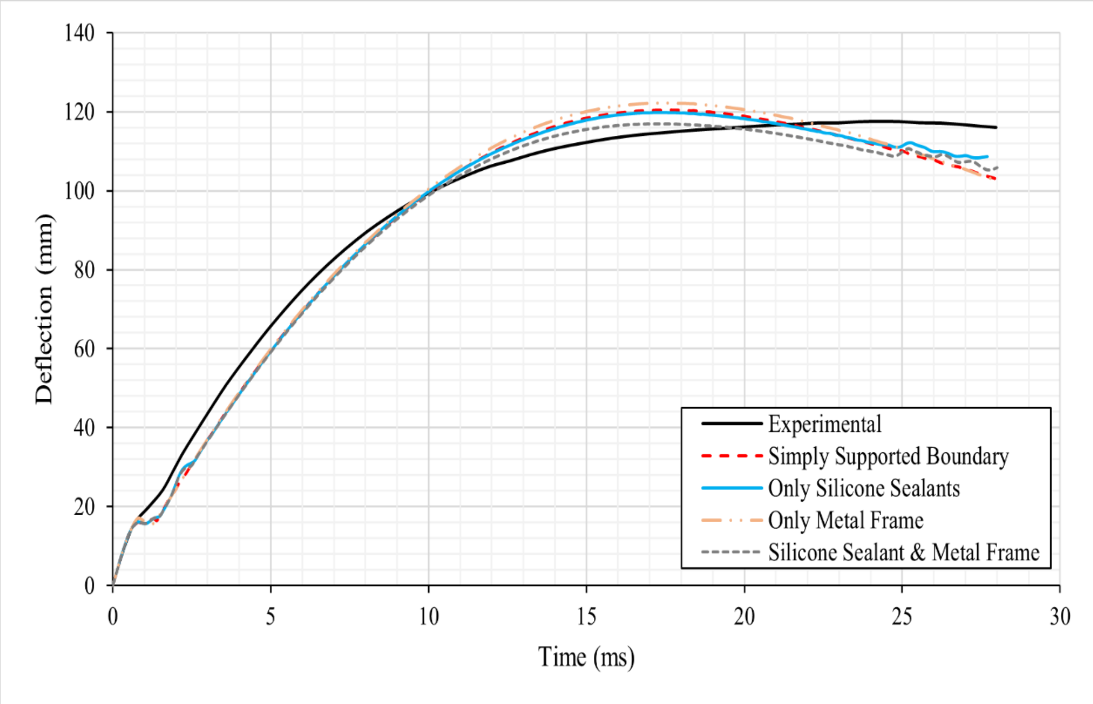

Fig. 4.2: Deflection time histories of LG panel with different boundary conditions

The experimental deflection-time history curve functions as the reference curve. The boundary condition of a simply supported structure successfully mirrors the initial deflection patterns; however, it falls short in accurately representing behaviour beyond the peak deflection phase. Silicone sealants tend to predict a slightly greater peak deflection than observed but correspond more closely to empirical data during the subsequent post-peak period. Although there are small deviations in the curves, both the simply supported panel and the panel supported with silicone sealant show similar overall behaviour, highlighting that the silicone sealant allows panel rotations comparable to simply supported boundaries. In contrast, the metal frame demonstrates a peak deflection that exceeds experimental observations, while its post-peak behaviour aligns with that of the simply supported condition, indicating a greater degree of rigidity and a diminished capacity for recovery. The integration of silicone sealants with a metal frame result in predictions that closely coincide with experimental results throughout both the peak deflection phase and the post-peak phase, effectively harmonizing characteristics of both rigidity and flexibility. Each boundary condition estimates a peak deflection near the experimental measurement of approximately 120 mm. Analysis of the recovery trends post-impact reveals that silicone sealants contribute to improved flexibility and recovery capabilities, whereas metal frames offer increased stiffness at the expense of reduced recovery.

Analysing the performance of glazing systems under impact loading is crucial for maintaining human safety across varied scenarios. Although Australian standards highlight the necessity for safety in glazing applications, they do not specifically analyse the influence of silicone sealants on the impact resistance of glass assemblies. In parallel, the AS/NZS 1170.2:2021 [7] standard addresses the dynamics of impact loading due to windborne debris as a component of wind actions, focusing on the structural design of glazing to withstand wind forces. Nonetheless, it does not distinctly evaluate how silicone sealants may enhance the impact resilience of these systems. This identified gap in the standards underscores the significance of accurately predicting energy absorption during rigid body impacts on LG, which is critical for assessing the comprehensive impact resistance of glazing systems. Such predictions are instrumental in assessing the protective efficacy of LG, particularly regarding human safety during impact scenarios. The energy absorption properties of various components within a LG unit including, the glass plies, interlayer, and surrounding frame, are depicted in Fig. 4.3.

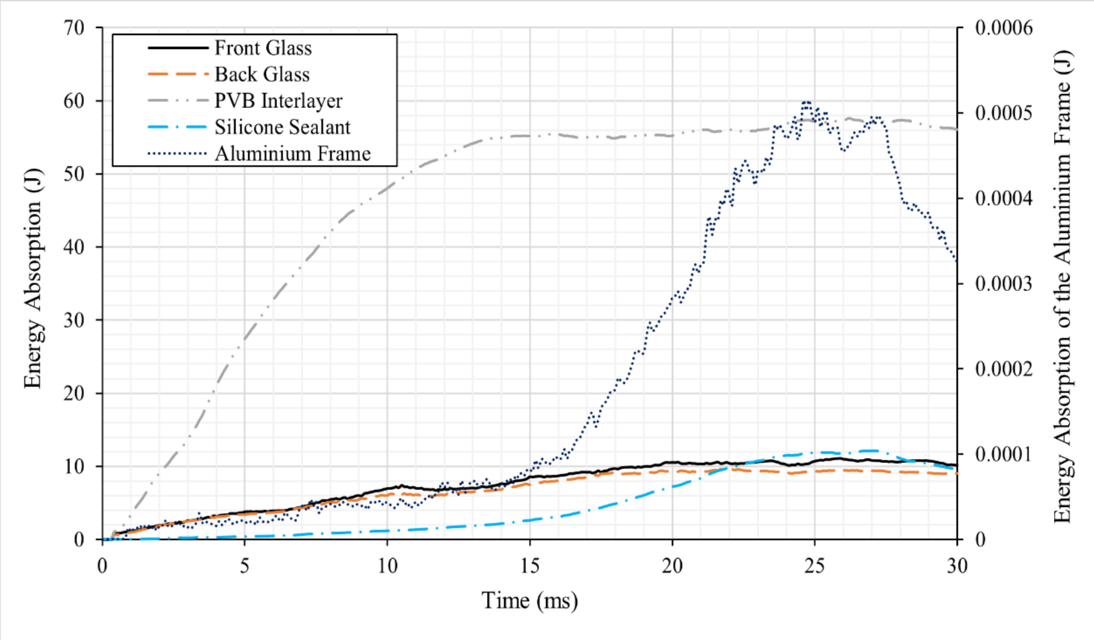

Fig. 4.3: Energy absorption of different components in LG unit system

The energy imparted by the projectile is distributed across several mechanisms: a portion facilitates the fracture and bending of the glass layers; another portion is engaged in the deformation and penetration of the interlayer material, while the remainder dissipates through the vibrations of the glass pane. Detailed analysis of energy absorption, depicted in Fig. 4.3, reveals that the PVB interlayer is the primary absorber of energy, accounting for roughly 70% of the total energy transferred. The front glass layer acts as a sacrificial barrier, absorbing about 12% of the energy, which is critical as it shatters upon impact to shield the internal environment from the projectile, thus alleviating stress on subsequent components [79]. The rear glass layer contributes to energy management by absorbing approximately 10%, aided by the cushioning properties of the interlayer [79]. Furthermore, the silicone sealant plays a pivotal role, accounting for 7.4% of total energy absorption, thereby enhancing both the system’s flexibility and its capacity for energy dissipation. This absorption is markedly greater compared to the minimal 0.000288% absorbed by the aluminium frame, which barely contributes to the overall energy dynamics.

Fig. 4.4 and Fig. 4.5 illustrate the variations in stress and the corresponding fracture patterns of the front glass panes in two distinct scenarios: aluminium frame without a silicone sealant (Fig 4.4) and aluminium frame with a silicone sealant layer (Fig 4.5), respectively. These cases are presented solely to demonstrate the influence and potential benefits of introducing a silicone sealant between the glass and the metal frame. The stress distributions are evaluated for maximum principal stress (first principal stress), second principal stress, and maximum shear (Tresca) stress over a 30 ms projectile impact duration. The findings indicate markedly higher stress concentrations in the frame without silicone sealant (Fig 4.4), with maximum principal stress reaching 25.2 MPa, while the second principal stress and maximum shear stress attain 10.3 MPa and 14.9 MPa, respectively.

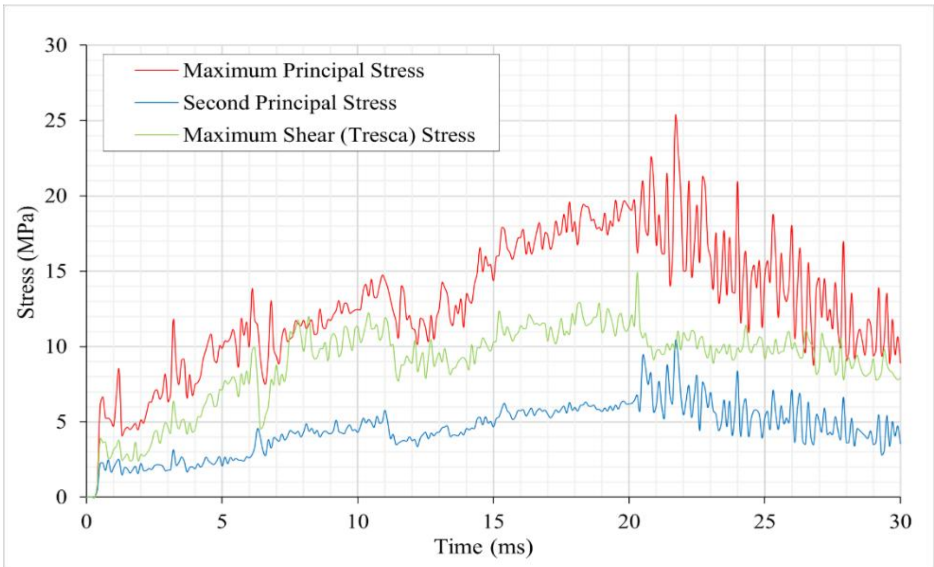

(a) Stress variations of aluminium frame under projectile impact

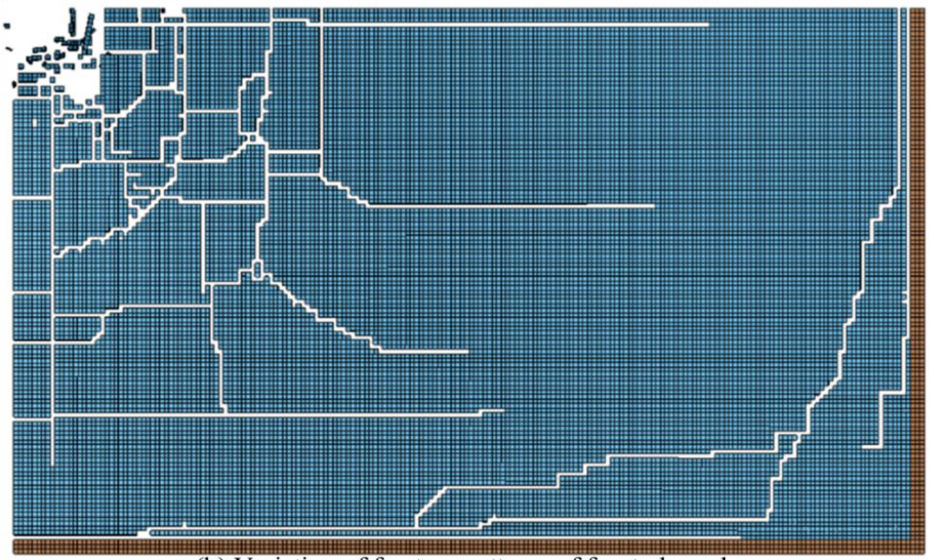

(b) Variation of fracture patterns of front glass ply

Fig. 4.4: Aluminium frame without silicone sealant

In contrast, the integration of silicone sealant significantly diminishes stress levels, achieving reductions exceeding 90% across all three stress variations. Without the silicone sealant layer, maximum stresses occur in a shorter time, whereas the addition of the silicone sealant enables the frame to absorb impact energy more effectively, delaying the occurrence of stress peaks in the metal frame. In Fig 4.4, the fracture density of the glass pane is significantly elevated near the frame due to heightened stress concentrations. Conversely, in Fig 4.5, the aluminium frame experiences reduced stress concentrations, as a greater proportion of the impact energy is absorbed by the silicone sealant rather than the aluminium frame (explained in Fig. 4.3). Consequently, the crack density near to the frame is reduced in Fig 4.5 relative to Fig 4.4 since the silicone sealant effectively absorbs and redistributes the impact energy, mitigating stress transfer to the aluminium frame.

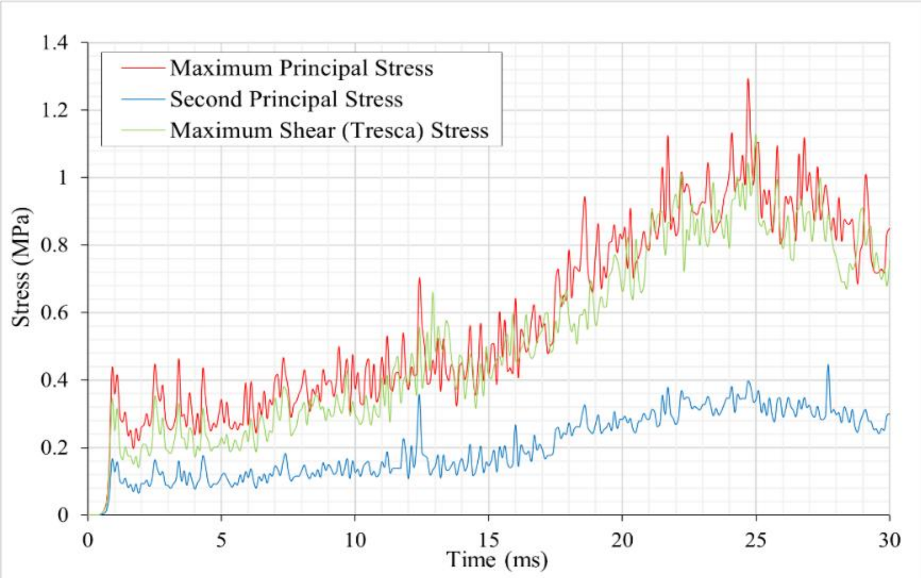

(a) Stress variations of aluminium frame under projectile impact

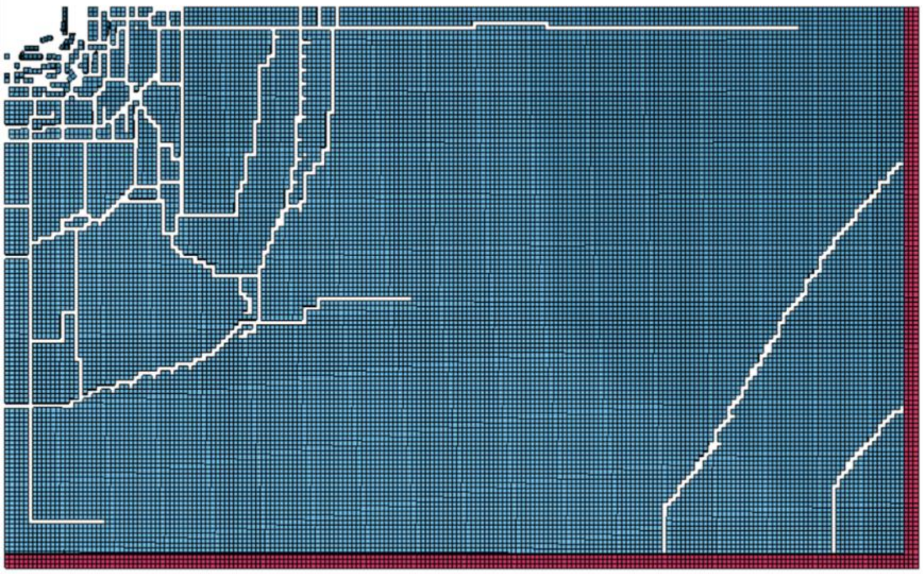

(b) Variation of fracture patterns of front glass ply

Fig. 4.5: Aluminium frame with silicone sealant

The insights derived from this study play a pivotal role in the development of LG systems capable of withstanding hurricane impacts. It has been identified that the PVB interlayer is more effective in deforming and dissipating energy upon impact compared to the glass plies. As elaborated in Section 3.2, augmenting the thickness of this interlayer substantially elevates its resistance to perforation. Similarly, the silicone sealant deserves careful optimization to maximize its energy absorption capabilities and sustain the integrity of the system. This approach not only enhances the system's flexibility in response to impact loads but also minimises the stress transfer to the building's primary structural frame. Consequently, a concentrated effort on refining both the interlayer and the silicone sealant are instrumental in markedly advancing the performance, resilience, and longevity of LG systems when subjected to extreme loading scenarios.

4.3 Development of Perforation Vulnerability Curves

By employing the validated FE model as detailed in Section 3, an investigation is performed on LG panels featuring four typical interlayer thicknesses: 1.52 mm, 1.88 mm, 2.28 mm, and 2.66 mm, to assess their vulnerability to perforation from a wooden projectile impact. These thicknesses are in line with ASTM standards [80]. To enhance computational efficiency, the model is studied exclusively under simply supported boundary conditions. The projectiles used in the study have masses of 2 kg, 4 kg, 6 kg, and 8 kg, with contact surface areas of 0.0025 m^2, 0.005 m^2, 0.0075 m^2, and 0.01 m^2. The projectile velocity varies from 5 m/s to 35 m/s, reflecting the potential peak speed of debris within cyclone region D [13]. Table 4.2 lists the critical thresholds for each combination of projectile mass, contact area, and velocity that result in perforation of LG panels with different interlayer thicknesses. Here, "N" signifies no perforation occurred, while "P" indicates perforation was observed.

Table 4.2: Perforation performance of LG (dimension of 2000 mm × 1200 mm)

Glass Thickness	PVB Thickness	Mass	2 kg	4 kg				6 kg	8 kg
		Contact Area	0.005 m^2	0.0025 m^2	0.005 m^2	0.0075 m^2	0.01 m^2	0.005 m^2	0.005 m^2
		Impact Velocity							
3 mm	1.52 mm	5 m/s	N	N	N	N	N	N	N
		7 m/s	N	N	N	N	N	N	N
		10 m/s	N	N	N	N	N	N	N
		12 m/s	N	N	N	N	N	N	P
		13 m/s	N	N	N	N	N	P	P

		15 m/s	N	P	N	N	N	P	P
		17 m/s	N	P	P	N	N	P	P
		19	N	P	P	N	N	P	P
		20 m/s	N	P	P	P	N	P	P
		25 m/s	P	P	P	P	P	P	P
		27 m/s	P	P	P	P	P	P	P
		30 m/s	P	P	P	P	P	P	P
		35 m/s	P	P	P	P	P	P	P
3 mm	1.88 mm	5 m/s	N	N	N	N	N	N	N
		7 m/s	N	N	N	N	N	N	N
		10 m/s	N	N	N	N	N	N	N
		13 m/s	N	N	N	N	N	N	N
		15 m/s	N	N	N	N	N	N	P
		16	N	P	N	N	N	N	P
		17 m/s	N	P	N	N	N	P	P
		20 m/s	N	P	P	N	N	P	P
		23 m/s	N	P	P	P	N	P	P
		25 m/s	N	P	P	P	P	P	P
		27 m/s	P	P	P	P	P	P	P
		30 m/s	P	P	P	P	P	P	P
		35 m/s	P	P	P	P	P	P	P
3 mm	2.28 mm	5 m/s	N	N	N	N	N	N	N
		7 m/s	N	N	N	N	N	N	N
		10 m/s	N	N	N	N	N	N	N
		13 m/s	N	N	N	N	N	N	N
		15 m/s	N	N	N	N	N	N	N
		17 m/s	N	P	N	N	N	N	P

		18	N	P	N	N	N	N	P
		20 m/s	N	P	N	N	N	P	P
		22	N	P	P	N	N	P	P
		25 m/s	N	P	P	P	N	P	P
		27 m/s	N	P	P	P	P	P	P
		30 m/s	N	P	P	P	P	P	P
		35 m/s	P	P	P	P	P	P	P
3 mm	2.66 mm	5 m/s	N	N	N	N	N	N	N
		7 m/s	N	N	N	N	N	N	N
		10 m/s	N	N	N	N	N	N	N
		13 m/s	N	N	N	N	N	N	N
		15 m/s	N	N	N	N	N	N	N
		17 m/s	N	N	N	N	N	N	N
		20 m/s	N	P	N	N	N	N	P
		25 m/s	N	P	N	N	N	P	P
		27 m/s	N	P	P	P	N	P	P
		30 m/s	N	P	P	P	P	P	P
		32 m/s	N	P	P	P	P	P	P
		35 m/s	P	P	P	P	P	P	P

Table 4.2 reveals that LG panels with interlayer thicknesses of 1.52 mm and 1.88 mm were able to resist perforation from a 4 kg wooden projectile travelling at 15 m/s (which corresponds to a momentum of 60 kg m/s), yet experienced perforation when hit by a 2 kg projectile at 30 m/s, although both projectiles had identical momentum. This trend is also evident for LG panels of the same thicknesses (1.52 mm and 1.88 mm), where impactors weighing 4 kg and 8 kg at velocities of 20 m/s and 10 m/s, respectively, lead to different perforation results under equivalent momentum. Moreover, LG panels with interlayer thicknesses of 2.28 mm and 2.66 mm could not prevent perforation from a 4 kg projectile at 30 m/s but successfully resisted an 8 kg projectile at 15 m/s, despite equivalent momentum in both scenarios. These observations suggest that equal momentum does not consistently result in the same

perforation outcome for LG panels. Additionally, an LG panel with a 1.52 mm interlayer thickness prevented perforation from a 4 kg projectile with a contact area of 0.005 m² at 15 m/s but did not when the contact area was halved to 0.0025 m² under the same mass and velocity circumstances. These findings imply that solely relying on impact momentum is inadequate to characterize LG's perforation potential. Instead, assessing perforation resistance requires considering the distinct effects of projectile mass, velocity, and contact area. Currently, there are no comprehensive guidelines for evaluating resistance of LG to debris impacts factoring in the projectile's mass, shape, and speed. Furthermore, given the complexities and costs associated with impact testing, creating vulnerability curves for LG panels is both difficult and costly.

Therefore, Fig. 4.6 and 4.7 showcase the perforation vulnerability curves derived from validated FE models, addressing aspects such as projectile mass, contact surface area, and impact velocity. Perforation was identified based on the complete penetration of the laminated glass system by the wooden impactor, accompanied by loss of load-carrying capacity and the formation of a through-thickness opening. These curves clarify the perforation occurrences for the LG panel specified in Table 4.2.

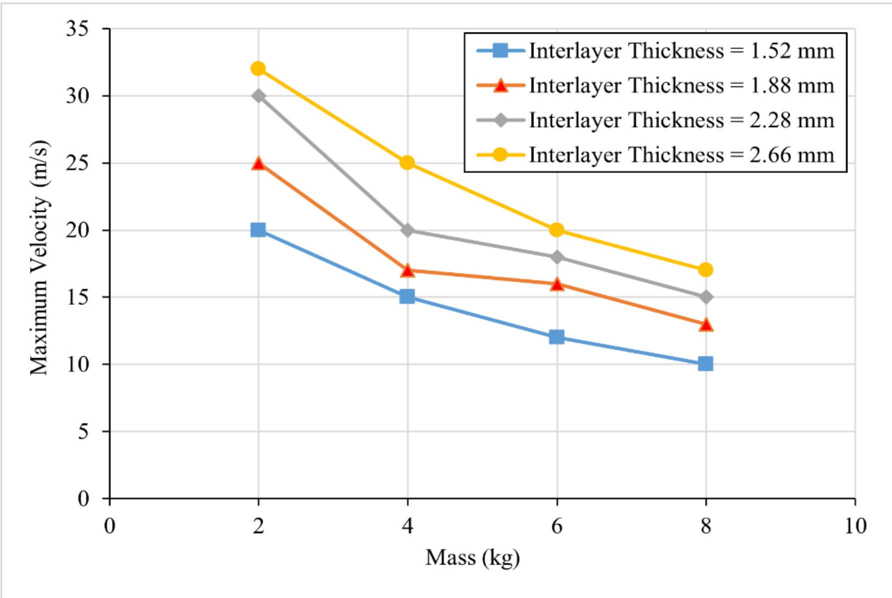

Fig. 4.6: Perforation vulnerability curve of LG related to projectile mass (dimension of 2000 mm × 1200 mm)

In Fig. 4.6, it is observed that perforation does not occur when the projectile's velocity and mass are located to the left and below the designated curve. Conversely, perforation is observed when these parameters are situated to the right and above the curve. It is anticipated that the LG exhibits a greater tendency for perforation when impacted by projectiles possessing larger masses and higher velocities.

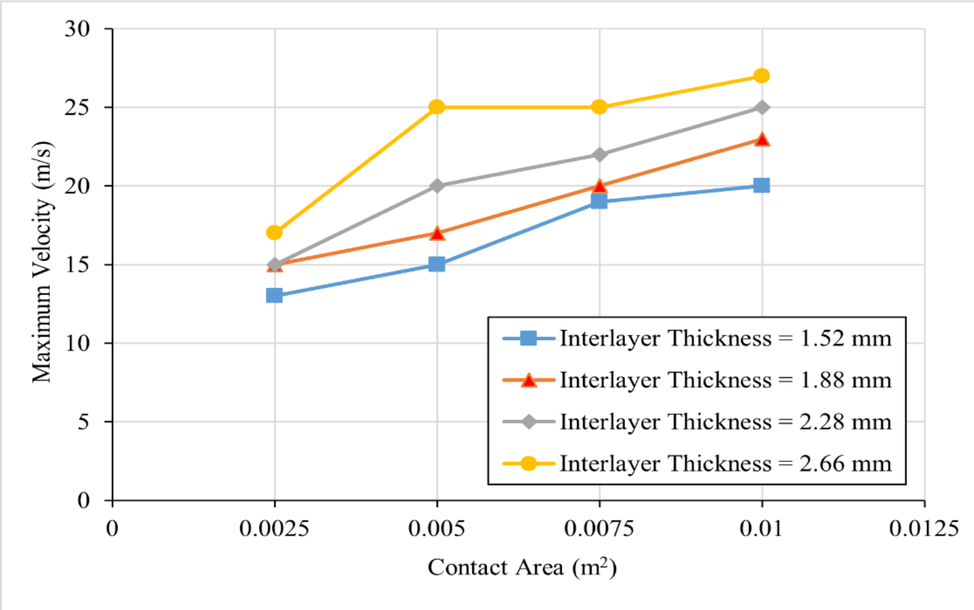

Fig. 4.7: Perforation vulnerability curve of LG related to the contact area of the projectile (dimension of 2000 mm × 1200 mm)

In Fig. 4.7, perforation does not happen when the projectile's velocity and contact surface area positioning are to the right and below the curve, while it occurs to the left and above the curve. As expected, LG exhibits greater susceptibility to perforation when struck by projectiles with reduced contact surface areas at increased velocities.

In both Fig. 4.6 and 4.7, an analysis reveals a consistent trend indicating that enhancing the perforation resistance capacity of the LG panel is achieved by incorporating a thicker interlayer. This specific approach to defining perforation resistance offers a more reliable assessment of the LG panel's ability to prevent perforation than the conventional assessment based on impact energy and momentum [52], [81]. Notably, these vulnerability curves may serve as an instrumental methodology for the evaluation and strategic design of LG panels, especially in reducing the adverse effects of projectile impacts, such as those resulting from windborne debris.

The study quantifies the efficiency of different interlayer thicknesses in preventing perforation by normalising impact velocities that cause perforation of a LG with those of an LG featuring a 1.52 mm thick interlayer. In Fig. 4.8, and similarly in Fig. 4.9, the graphs illustrate how the normalised velocity correlates with interlayer thickness. This relationship is analysed for four distinct projectile masses: 2 kg, 4 kg, 6 kg, and 8 kg, alongside four varying contact surface areas: 0.0025 m², 0.005 m², 0.0075 m², and 0.01 m², which were systematically explored throughout the present investigation.

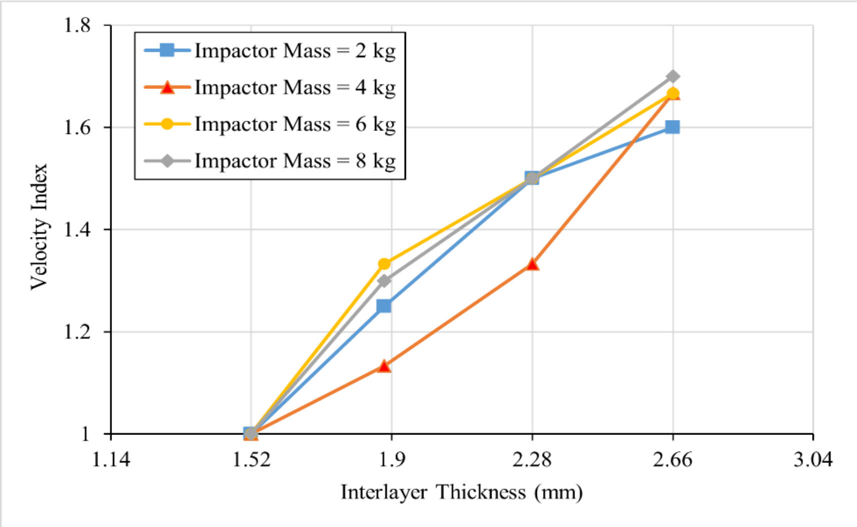

Fig.4.8. Effectiveness of the PVB interlayer thickness on perforation resistance (related to mass of the projectile)

As demonstrated in Fig. 4.8, increasing the thickness of the interlayer significantly enhances the capacity of the glass to resist perforation. Specifically, when the interlayer thickness is increased from 1.52 mm to 2.66 mm, there is a notable 60% enhancement in the perforation resistance of a LG panel with dimensions of 2000 mm by 1200 mm when subjected to the impact of a 2 kg wooden projectile. This improvement in perforation resistance is even more substantial when the glass is exposed to impacts by projectiles of larger mass. For instance, elevating the interlayer thickness from 1.52 mm to 2.66 mm results in an approximately 66.7% increase in the resistance capacity of the LG panel against 4 kg and 6 kg projectiles, while for an 8 kg projectile, the resistance capacity increases by roughly 70%. In further detail, for an 8 kg projectile to successfully perforate the LG with an interlayer thickness of 2.66 mm, the required impact velocity must surpass 1.7 times the velocity needed to achieve perforation in glass with an interlayer that is 1.52 mm thick.

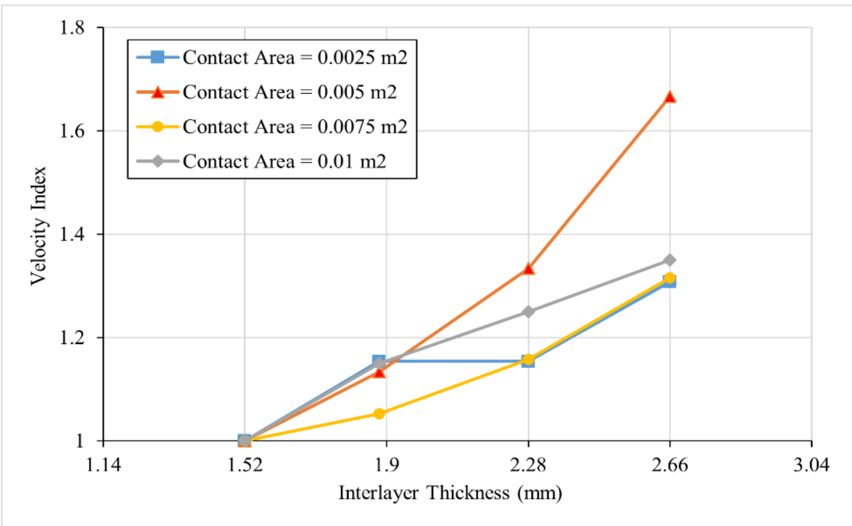

Fig.4.9: Effectiveness of the PVB interlayer thickness on perforation resistance (related to contact area of the projectile)

Fig. 4.9 demonstrates that significantly increasing the interlayer thickness in LG panels robustly enhances their resistance to perforation, with this improvement becoming more pronounced as the contact area enlarges. In scenarios where the contact area is relatively small, at 0.0025 m^2, raising the interlayer thickness from 1.52 mm to 2.66 mm results in a moderate improvement in resistance, which is quantifiable by a 30.8% increase in the velocity index. When considering a moderate contact area of 0.005 m^2, the resistance enhancement becomes noticeably more significant, achieving a 66.7% increase with the same adjustment in thickness. For contact areas of 0.0075 m^2 and 0.01 m^2, the improvement effects are approximately 31% and 35% respectively, indicating a consistent yet substantial enhancement. These results suggest that increasing interlayer thickness is particularly effective for moderate to large contact areas, while presenting relatively modest improvements for smaller contact areas such as those measuring 0.0025 m^2. Thus, incorporating thicker interlayers is most beneficial in scenarios where impacts with extensive surface areas are anticipated. The enhancement in the panels' penetration resistance is dependent on the contact area, peaking in its effectiveness at moderate values such as 0.005 m^2. This implies that LG design should strategically account for the expected impact contact area relevant to specific applications, for example, impacts from storm debris or ballistic threats. Though increasing interlayer thickness consistently boosts resistance, it also contributes additional weight. Hence, designers must navigate the trade-off between increased weight and enhanced protection to ensure the practicality of LG in applications spanning transportation, architectural glazing, and windows designed to withstand storms.

Upon examining Fig. 4.8 and 4.9, it becomes evident that enlarging the contact area of the impactor proves to be more efficacious in reducing the susceptibility of glass panels to perforation than merely reducing the impactor's mass. This observation suggests that widened surface interactions play a crucial role in diminishing the likelihood of perforation by facilitating a more widespread distribution of impact forces across the glass panel.

CHAPTER 5

CONCLUSIONS

5.1 Summary and Main Findings of the Research

This research developed and validated a high-fidelity finite element (FE) model to evaluate the impact resistance of laminated glass (LG) panels subjected to wood block projectiles, as specified in standard impact testing guidelines. The model incorporated dynamically calibrated Johnson-Holmquist Ceramic (JH-2) material parameters for float glass, derived through a rigorous meta-analysis of recent literature. Benchmarking against experimental data demonstrated strong agreement across key performance indicators, namely deflection time histories, peak displacements, maximum strains, stress distributions, and fracture patterns, affirming the robustness of the proposed modelling approach. Statistical validation further confirmed the model's accuracy compared to existing numerical studies, providing confidence in its predictive capabilities.

The validated FE framework was systematically expanded to simulate over 276 different impact scenarios involving variations in interlayer thickness (1.52 mm, 1.88 mm, 2.28 mm, and 2.66 mm), projectile mass (2 kg, 4 kg, 6 kg, and 8 kg), and contact area (0.0025 m^2, 0.005 m^2, 0.0075 m^2, and 0.01 m^2), addressing a critical gap in existing literature where such breadth of analysis has been constrained by the prohibitive cost and logistics of full-scale physical testing.

These simulations revealed several key insights into the energy dissipation mechanisms within the selected laminated glass (LG) system comprising a 2000 mm × 1200 mm panel with 3 mm glass plies and a 1.88 mm PVB interlayer. The front glass ply acted predominantly as a sacrificial layer, absorbing about 12% of the impact energy through radial and circumferential cracking. In contrast, the back glass ply failed under bending-induced tensile stresses, absorbing approximately 10% of the impact energy, aided by the cushioning effect of the PVB interlayer. Notably, the PVB interlayer was identified as the primary energy absorber, absorbing the majority of the impact energy (70% of the impact energy) through its viscoelastic deformation. These observations are specific to the investigated configuration, as the glass and interlayer thicknesses were not varied in this study. An increase in glass thickness would be expected to enhance energy absorption within the glass plies, thereby reducing the energy transferred to the interlayer.

In contrast to earlier computational analyses that neglected to incorporate silicone sealant, this investigation explicitly incorporated it in the simulation between the glass and aluminium frame, revealing that its presence contributed to a substantial reduction in stress levels of the supporting frame exceeding 90% with respect to the maximum principal stress, second principal stress, and maximum shear stress values. Furthermore, the silicone sealant was instrumental in postponing the occurrence of peak stresses within the metal frame, thereby enabling a more effective redistribution of impact energy, which subsequently led to a decrease in stress concentrations and a decrease in crack density proximate to the periphery of the LG panel.

The research also involved the creation of perforation vulnerability curves specifically tailored for an LG panel with dimensions of 2000 mm by 1200 mm. These curves were instrumental in evaluating the influence of several variables, namely the interlayer thickness, the mass of the projectile, and the projectile's point of contact area, on the perforation resistance capabilities of the LG panel. Evidence from the study indicated that relying solely on impact momentum as a determinant for perforation resistance is inadequate. It is imperative to account for the distinct roles played by projectile mass, its velocity, and the area of contact when assessing perforation resistance. Interestingly, it was observed that a reduction in the impactor's contact area has a more detrimental effect on perforation resistance than an increase in the impactor's mass. Therefore, these parameters must be carefully considered together for a comprehensive understanding of the perforation performance of LG panels.

The outcome of this research not only advances the state-of-the-art in impact modelling of glazing systems but also provided a practical design framework for performance-based assessments of LG panels. Applications included hurricane-resistance facades, security glazing, and other scenarios demanding high-impact resilience, where these insights can guide more effective and economical design strategies.

5.2 Recommendations for Future Research

While this study has addressed several key limitations in the existing literature and delivered a validated framework for the impact analysis of LG, it also opens new avenues for research that can further enrich the field:

- The current model had not considered thermal effects. However, real-world environments introduce temperature fluctuations that influence the mechanical and viscoelastic behaviour of PVB interlayers. Incorporating thermos-mechanical coupling into future FE models would enable more realistic performance evaluations under environmental loading scenarios.

- The scarcity of publicly available experimental data limited broader validation. Further efforts should focus on generating additional high-quality experimental results across various impact conditions, glass configurations, and environmental settings to support more comprehensive model benchmarking.

- In the existing literature, delamination behaviour is not explicitly reported for the tested laminated glass panels. Nevertheless, such behaviour should be examined thoroughly in the future experimental studies, as higher impact energies or repeated debris impacts may induce interfacial debonding. The occurrence of delamination could significantly alter stress transfer mechanisms and energy dissipation within the laminate. Consequently, explicit modelling of glass-interlayer debonding should be explored to quantify its influence and address this limitation of the current framework.

- Architectural applications often employ curved LG, which introduces geometric nonlinearities and complex stress distributions under impact. Further studies should explore both experimental and numerical analyses on curved LG panels to extend the applicability of current models.

- The perforation vulnerability curves developed here were specific to a certain panel size and glass type. Future research should aim to expand this framework across a broader spectrum of geometries, glazing compositions, and interlayer materials to build a more generalised design tool.

- The present analysis focused exclusively on central impact scenarios. In practice, corner and edge impacts may be more critical due to reduced structural restraint and stress concentration effects. Future studies should systematically compare central, edge, and corner impacts to establish governing failure modes and identify the most critical loading scenarios for design.

- The damage accumulation rate parameter (D_1) in the JH-2 material model plays a critical role in simulating brittle fracture. As noted in the LS-DYNA manual, D_1 is the most effective parameter for aligning simulation results across software platforms. A parametric sensitivity study focusing on D_1 would provide deeper insights into model tuning and transferability.

- With the extensive numerical dataset generated in this study, there is significant potential for developing machine learning (ML) models to enable rapid predictions of impact outcomes. Such surrogate models could facilitate real-time assessment and be integrated into design optimisation workflows, reducing the computational cost of traditional FE simulations.

Addressing these research directions will enhance the fidelity, applicability, and efficiency of impact performance model for LG systems, thereby contributing to the broader objective of safer and more resilient built environments.

REFERENCES

[1] C. Bedon, X. Zhang, F. Santos, D. Honfi, M. Kozlowski, M. Arrigoni, L. Figuli, D. Lange, "Performance of structural glass facades under extreme loads – Design methods, existing research, current issues and trends," Construction and Building Materials, vol. 163, pp. 921–937, 2018, doi: 10.1016/j.conbuildmat.2017.12.153.

[2] H. D. Hidallana-Gamage, D. P. Thambiratnam, and N. J. Perera, "Failure analysis of laminated glass panels subjected to blast loads," Engineering Failure Analysis, vol. 36, pp. 14–29, Jan. 2014, doi: 10.1016/j.engfailanal.2013.09.018.

[3] X. Zhang, H. Hao, and G. Ma, "Laboratory test and numerical simulation of laminated glass window vulnerability to debris impact," International Journal of Impact Engineering, vol. 55, pp. 49–62, May 2013, doi: 10.1016/j.ijimpeng.2013.01.002.

[4] M. Nawar, H. Salim, M. Newberry, and A. El-Sisi, "High strain rate response of laminated glass interlayer materials," Construction and Building Materials, vol. 299, p. 123934, Sep. 2021, doi: 10.1016/j.conbuildmat.2021.123934.

[5] N. D. Kaiser, R. A. Behr, J. E. Minor, L. R. Dharani, F. Ji, and P. A. Kremer, "Impact Resistance of Laminated Glass Using 'Sacrificial Ply' Design Concept," Journal of Architectural Engineering, vol. 6, no. 1, pp. 24–34, Mar. 2000, doi: 10.1061/(ASCE)1076-0431(2000)6:1(24).

[6] M. Timmel, S. Kolling, P. Osterrieder, and P. A. Du Bois, "A finite element model for impact simulation with laminated glass," International Journal of Impact Engineering, vol. 34, no. 8, pp. 1465–1478, Aug. 2007, doi: 10.1016/j.ijimpeng.2006.07.008.

[7] Structural design actions, Part 2: Wind actions. AS/NZS 1170.2. Australian/New Zealand Standard, 2021, Available: https://www.standards.govt.nz/shop/asnzs-1170-22021

[8] Standard Test Method for Performance of Exterior Windows, Curtain Walls, Doors, and Impact Protective Systems Impacted by Missile(s) and Exposed to Cyclic Pressure Differentials. ASTM E1886-19. West Conshohocken, Pennsylvania, United States: ASTM International, 2019, doi: 10.1520/E1886-19

[9] Standard Specification for Performance of Exterior Windows, Curtain Walls, Doors, and Impact Protective Systems Impacted by Windborne Debris in Hurricanes. ASTM E1996-23. West Conshohocken, Pennsylvania, United States: ASTM International, 2023, doi: 10.1520/E1996-23.

[10] J. R. McDonald, J. E. Minor, and K. C. Mehta, "Interim Guidelines for Building Occupant Protection from Tornadoes and Extreme Winds," United States Government Printing Office, Sep. 1975, Available: http://hdl.handle.net/1969.3/27090

[11] X. Zhang, H. Hao, and G. Ma, "Dynamic material model of annealed soda-lime glass," International Journal of Impact Engineering, vol. 77, pp. 108–119, Mar. 2015, doi: 10.1016/j.ijimpeng.2014.11.016.

[12] X.-Q. Zhou, M.-Y. Wang, and L.-X. Li, "Dynamic damage assessment of float glass under blast loading," Advances in Structural Engineering, vol. 22, no. 11, pp. 2517–2529, Aug. 2019, doi: 10.1177/1369433219845691.

[13] Structural design actions, Part 2: Wind actions. AS/NZS 1170.2. Australian/New Zealand Standard, 2011. Available: https://www.standards.govt.nz/shop/asnzs-1170-22011

[14] M. Achintha, “Sustainability of glass in construction,” in Sustainability of Construction Materials (Second Edition), Woodhead Publishing Series in Civil and Structural Engineering, pp. 79-104, 2016, doi: 10.1016/B978-0-08-100370-1.00005-6.

[15] S. T. Akter and M. Khani, "Characterisation of laminated glass for structural applications," Linnaeus University, Faculty of Technology, Department of Building and Energy Technology, 2013, Available: https://www.diva-portal.org/smash/record.jsf?pid=diva2%3A627177&dswid=9852.

[16] K. C. Datsiou, “Bioinspired improvement of laminated glass,” Science, vol. 364, no. 6447, pp. 1232–1233, Jun. 2019, doi: 10.1126/science.aax9677 .

[17] M. Martín, X. Centelles, A. Solé, C. Barreneche, A. I. Fernández, and L. F. Cabeza, “Polymeric interlayer materials for laminated glass: A review,” Construction and Building Materials, vol. 230, Jan. 2020, doi: 10.1016/j.conbuildmat.2019.116897.

[18] L. Biolzi, S. Cattaneo, M. Orlando, L. R. Piscitelli, and P. Spinelli, “Post-failure behavior of laminated glass beams using different interlayers,” Composite Structures, vol. 202, pp. 578–589, Oct. 2018, doi: 10.1016/j.compstruct.2018.03.009.

[19] G. D’Ambrosio, L. Galuppi, and G. Royer-Carfagni, “Post-breakage in-plane stiffness of laminated glass: an engineering approach,” Glass Structures and Engineering, vol. 4, pp. 421–432, Oct. 2019, doi: 10.1007/s40940-019-00099-1.

[20] C. Kranzer, G. Gürke, and C. Mayrhofer, “Testing of bomb resistant glazing systems experimental investigations of the time dependent deflection of blast loaded 7.5 mm laminated glass,” presented at the Glass Processing Days (GPD) 2005, 2005, Available: https://publica.fraunhofer.de/handle/publica/348274

[21] K. A. D. L. P. Karunarathna, “Low-velocity impact analysis of monolithic and laminated glass using finite element method (FEM),” MSc Thesis, University of Birmingham, Birmingham, United Kingdom, 2013, Available: http://etheses.bham.ac.uk/id/eprint/5067

[22] H. D. Hidallana-Gamage, “Response of Laminated Glass Panels to Near Field Blast Events,” PhD Thesis, Queensland University of Technology, Queensland, Australia, 2015, Available: https://eprints.qut.edu.au/85263/

[23] T. W. M. C. Wanigasooriya, H. D. Hidallana-Gamage, and K. Baskaran, “Development of a Finite Element Model of Glass Balustrade Under Soft Body Impact Test,” in 2024 Moratuwa Engineering Research Conference (MERCon), Aug. 2024, pp. 682–687. doi: 10.1109/MERCon63886.2024.10688947.

[24] V. Silberschmidt, "Dynamic Deformation, Damage and Fracture in Composite Materials and Structures". Woodhead Publishing Series in Composites Science and Engineering, 2023, doi: 10.1016/C2020-0-01086-8.

[25] M. E. Backman and W. Goldsmith, “The mechanics of penetration of projectiles into targets,” International Journal of Engineering Science, vol. 16, no. 1, pp. 1–99, Jan. 1978, doi: 10.1016/0020-7225(78)90002-2.

[26] A. Ball and H. W. McKenzie, “On the low velocity impact behaviour of glass plates,” Journal de Physique IV, vol. 04, no. C8, pp. 783-788, Sep. 1994, doi: 10.1051/jp4:19948121.

[27] T. Børvik, “Ballistic Penetration and Perforation of Steel Plates,” Doctoral thesis, Fakultet for ingeniørvitenskap og teknologi, 2001, Available: https://ntnuopen.ntnu.no/ntnu-xmlui/handle/11250/236412

[28] J. A. Zukas, “Impact Dynamics: Theory and Experiment,” US Army Ballistic Research Laboratory, Aberdeen Proving Ground, Maryland, 1982, Available: https://apps.dtic.mil/sti/citations/ADA093502

[29] R. S. J. Corran, P. J. Shadbolt, and C. Ruiz, “Impact loading of plates - An experimental investigation,” International Journal of Impact Engineering, vol. 1, no. 1, pp. 3-22, Jan. 1983, doi: 10.1016/0734-743X(83)90010-6.

[30] W. Goldsmith and J. T. Frasier, “Impact: The Theory and Physical Behavior of Colliding Solids,” Journal of Applied Mechanics, vol. 28, no. 4, Dec. 1961, doi: 10.1115/1.3641808.

[31] P. Hála, A. Zemanová, J. Zeman, and M. Šejnoha, “Numerical study on failure of laminated glass subjected to low-velocity impact,” Glass Structures & Engineering, vol. 8, pp. 99-117, Oct. 2022, doi: 10.1007/s40940-022-00210-z.

[32] A. Zemanová, P. Hála, P. Konrád, J. Schmidt, R. Sovják, and M. Šejnoha, “On the Low-Velocity Impact Response of Laminated Glass with Different Types of Glass and Interlayers,” Challenging Glass Conference Proceedings, vol. 7, Sep. 2020, doi: 10.7480/CGC.7.4483.

[33] A. Zemanová, P. Hála, P. Konrád, R. Sovják, and M. Šejnoha, “Gradual fracture of layers in laminated glass plates under low-velocity impact,” Computers & Structures, vol. 283, Jul. 2023, doi: 10.1016/j.compstruc.2023.107053.

[34] J.-C. Liu, S.-G. Yang, Y. Yang, Q. Fang, C. Rong, and J.-P. Gan, “Experimental study of the dynamic response of PVB laminated glass under vented explosion loads of methane–air mixtures,” International Journal of Impact Engineering, vol. 143, Sep. 2020, doi: 10.1016/j.ijimpeng.2020.103588.

[35] X. Wang, J. Yang, Q. Liu, Y. Zhang, and C. Zhao, “A comparative study of numerical modelling techniques for the fracture of brittle materials with specific reference to glass,” Engineering Structures, vol. 152, pp. 493–505, Dec. 2017, doi: 10.1016/j.engstruct.2017.08.050.

[36] X. Wang, J. Yang, F. Wang, Q. Liu, and H. Xu, “Simulating the impact damage of laminated glass considering mixed mode delamination using FEM/DEM,” Composite Structures, vol. 202, pp. 1239–1252, Oct. 2018, doi: 10.1016/j.compstruct.2018.05.127.

[37] X. Wang, J. Yang, Q. Liu, and C. Zhao, “Experimental investigations into SGP laminated glass under low velocity impact,” International Journal of Impact Engineering, vol. 122, pp. 91–108, Dec. 2018, doi: 10.1016/j.ijimpeng.2018.06.010.

[38] Technical Note 4 - Simulated Windborne Debris Impact Testing of Building Envelope Components. James Cook University, Townsville, QLD 4811, Australia, 2011.

[39] G. Belingardi and R. Vadori, “Low velocity impact tests of laminate glass-fiber-epoxy matrix composite material plates,” International Journal of Impact Engineering, vol. 27, no. 2, pp. 213–229, Feb. 2002, doi: 10.1016/S0734-743X(01)00040-9.

[40] L. Aretxabaleta, J. Aurrekoetxea, I. Urrutibeascoa, and M. Sánchez-Soto, “Characterisation of the impact behaviour of polymer thermoplastics,” Polymer Testing, vol. 24, no. 2, pp. 145–151, Apr. 2005, doi: 10.1016/j.polymertesting.2004.09.014.

[41] Y. Liu and B. Liaw, “Drop-weight impact tests and finite element modeling of cast acrylic/aluminum plates,” Polymer Testing, vol. 28, no. 8, pp. 808–823, Dec. 2009, doi: 10.1016/j.polymertesting.2009.07.003.

[42] S. Zhu and G. B. Chai, “Ductile and Brittle Material Failures in Low-Velocity Impact,” Proceedings of the Institution of Mechanical Engineers, Part L: Journal of Materials: Design and Applications, vol. 224, no. 4, pp. 162–172, Oct. 2010, doi: 10.1243/14644207JMDA327.

[43] F. B. Langitan and B. R. Lawn, “Hertzian Fracture Experiments on Abraded Glass Surfaces as Definitive Evidence for an Energy Balance Explanation of Auerbach’s Law,” Journal of Applied Physics, vol. 40, no. 10, pp. 4009–4017, Sep. 1969, doi: 10.1063/1.1657136.

[44] S. M. Wiederhorn and B. R. Lawn, “Strength Degradation of Glass Resulting from Impact with Spheres,” Journal of the American Ceramic Society, vol. 60, pp. 451–458, 1977, doi: 10.1111/j.1151-2916.1977.tb15531.x.

[45] H. P. Kirchner and R. M. Gruver, “Localized impact damage in glass,” Materials Science and Engineering, vol. 28, no. 1, pp. 153–160, Apr. 1977, doi: 10.1016/0025-5416(77)90099-4.

[46] A. Ball, “The Low Velocity Impact Behaviour of Glass-Polymer Laminated Plates,” Journal de Physique IV, vol. 07, no. C3, pp. C3-926, Aug. 1997, doi: 10.1051/jp4:19973155.

[47] P. V. Grant, W. J. Cantwell, H. McKenzie, and P. Corkhill, “The Damage Threshold of Laminated Glass Structures,” International Journal of Impact Engineering, vol. 21, no. 9, pp. 737–746, Oct. 1998, doi: 10.1016/S0734-743X(98)00027-X.

[48] P. V. Grant and W. J. Cantwell, “Impact failure modes in glass structures,” Proceedings of the Institution of Mechanical Engineers, Part D: Journal of Automobile Engineering, vol. 213, no. 6, pp. 519–529, Jun. 1999, doi: 10.1243/0954407991527071.

[49] A. I. Shutov, A. N. Frank, I. A. Novikov, A. S. Ostapko, A. S. Bonchuk, and A. N. Burdov, “Testing Laminated Glass for Impact Resistance,” Glass and Ceramics, vol. 61, no. 3, pp. 67–69, Mar. 2004, doi: 10.1023/B:GLAC.0000034048.79421.08.

[50] W. L. Beason, G. E. Meyers, and R. W. James, “Hurricane Related Window Glass Damage in Houston,” Journal of Structural Engineering, vol. 110, no. 12, pp. 2843–2857, Dec. 1984, doi: 10.1061/(ASCE)0733-9445(1984)110:12(2843).

[51] P. L. Harris, “The effects of thickness and temper on the resistance of glass to small missile impact,” MSc Thesis, Texas Tech University, USA, 1978, Available: http://hdl.handle.net/2346/20288

[52] S. A. Bole, “Investigation of the Mechanics of Windborne Missile Impact on Window Glass,” MSc Thesis, Texas Tech University, USA, 1999, Available: http://hdl.handle.net/2346/62122

[53] N. Kishi and A. Q. Bhatti, “An equivalent fracture energy concept for nonlinear dynamic response analysis of prototype RC girders subjected to falling-weight impact loading,” International Journal of Impact Engineering, vol. 37, no. 1, pp. 103-113, Jan. 2010, doi: 10.1016/j.ijimpeng.2009.07.007.

[54] B. Liu, R. Villavicencio, and C. Guedes Soares, “Experimental and numerical plastic response and failure of pre-notched transversely impacted beams,” International Journal of Mechanical Sciences, vol. 77, pp. 314-332, Dec. 2013, doi: 10.1016/j.ijmecsci.2013.09.032.

[55] H. N. Dhakal, Z. Y. Zhang, N. Bennett, and P. N. B. Reis, “Low-velocity impact response of non-woven hemp fibre reinforced unsaturated polyester composites: Influence of impactor geometry and impact velocity,” Composite Structures, vol. 94, no. 9, pp. 2756-2763, Sep. 2012, doi: 10.1016/j.compstruct.2012.04.004.

[56] S. M. R. Khalili, M. Soroush, A. Davar, and O. Rahmani, “Finite element modeling of low-velocity impact on laminated composite plates and cylindrical shells,” Composite Structures, vol. 93, no. 5, pp. 1363–1375, Apr. 2011, doi: 10.1016/j.compstruct.2010.10.003.

[57] R. Poola, “Bird strike impact analysis of vertical stabilizer structure using abaqus/explicit,” presented at the SIMULIA India Regional Users Meeting, Bengaluru, 2011.

[58] J. Oda and M. Y. Zang, “Analysis of Impact Fracture Behavior of Laminated Glass of Bi-Layer Type Using Discrete Element Method,” Key Engineering Materials, vol. 145-149, pp. 349-354, Oct. 1997, doi: 10.4028/www.scientific.net/KEM.145-149.349.

[59] F. W. Flocker and L. R. Dharani, “Low Velocity Impact Resistance of Laminated Architectural Glass,” Journal of Architectural Engineering, vol. 4, no. 1, pp. 12-17, Mar. 1998, doi: 10.1061/(ASCE)1076-0431(1998)4:1(12).

[60] F. W. Flocker and L. R. Dharani, “Stresses in laminated glass subject to low velocity impact,” Engineering Structures, vol. 19, no. 10, pp. 851–856, Oct. 1997, doi: 10.1016/S0141-0296(97)00162-4.

[61] F. W. Flocker and L. R. Dharani, “Modelling fracture in laminated architectural glass subject to low velocity impact,” Journal of Materials Science, vol. 32, pp. 2587-2594, May 1997, doi: 10.1023/A:1018698900942.

[62] C. D. Wu, X. Q. Yan, and L. M. Shen, “A numerical study on dynamic failure of nanomaterial enhanced laminated glass under impact,” IOP Conference Series: Materials Science and Engineering, vol. 10, Jun. 2010, doi: 10.1088/1757-899X/10/1/012176.

[63] M. Y. Zang, H. Chen, and Z. Lei, “Simulation on High Velocity Impact Process of Windshield by SPH/FEM Coupling Method,” in 2010 WASE International

Conference on Information Engineering, pp. 381-384, Aug. 2010, doi: 10.1109/ICIE.2010.268.

[64] G. R. Johnson and T. J. Holmquist, "An improved computational constitutive model for brittle materials," in AIP Conference Proceedings, Colorado Springs, Colorado (USA): AIP, pp. 981-984, 1994, doi: 10.1063/1.46199.

[65] T. J. Holmquist, G. R. Johnson, C. M. Lopatin, D. E. Grady, and E. S. Hertel Jr, "High Strain Rate Properties and Constitutive Modeling of Glass," presented at the 15th International Symposium on Ballistics, Jerusalem, Israel, May 1995, doi: 10.2172/41367

[66] H. D. Hidallana-Gamage, D. P. Thambiratnam, and N. J. Perera, "Numerical modelling and analysis of the blast performance of laminated glass panels and the influence of material parameters," Engineering Failure Analysis, vol. 45, pp. 65–84, Oct. 2014, doi: 10.1016/j.engfailanal.2014.06.013.

[67] W. C. Brown, "A practicable formulation for the strength of glass and its special application to large plates," National Research Council of Canada. Institute for Research in Construction, Aug. 1970, doi: 10.4224/23002290.

[68] M. Peroni, G. Solomos, V. Pizzinato, and M. Larcher, "Experimental Investigation of High Strain-Rate Behaviour of Glass," Applied Mechanics and Materials, vol. 82, pp. 63-68, Jul. 2011, doi: 10.4028/www.scientific.net/AMM.82.63.

[69] N. K. Bourne, J. C. F. Millett, and J. E. Field, "On the strength of shocked glasses," Proceedings of the Royal Society A, vol. 455, no. 1984, pp. 1275–1282, Apr. 1999, doi: 10.1098/rspa.1999.0360.

[70] R. Feng, "Formation and propagation of failure in shocked glasses," Journal of Applied Physics, vol. 87, no. 4, pp. 1693–1700, Feb. 2000, doi: 10.1063/1.372079.

[71] M. J. Meyland and J. H. Nielsen, "Ongoing Research into the Failure of Glass at High Strain-Rates," Challenging Glass Conference Proceedings, vol. 7, Sep. 2020, doi: 10.7480/CGC.7.4428.

[72] Wenyu Cheng, X. Hu, and H. Pan, "Johnson–Holmquist Model Parameter Determination for Tempered Glass under Impact Loading," Glass Physics and Chemistry, vol. 49, no. 4, pp. 340-353, Aug. 2023, doi: 10.1134/S1087659622600193.

[73] H. D. Hidallana-Gamage, D. P. Thambiratnam, and N. J. Perera, "Influence of interlayer properties on the blast performance of laminated glass panels," Construction and Building Materials, vol. 98, pp. 502–518, Nov. 2015, doi: 10.1016/j.conbuildmat.2015.08.129.

[74] R. Iwasaki, C. Sato, J. L. Latailladeand, and P. Viot, "Experimental study on the interface fracture toughness of PVB (polyvinyl butyral)/glass at high strain rates," International Journal of Crashworthiness, vol. 12, no. 3, pp. 293–298, Sep. 2007, doi: 10.1080/13588260701442249.

[75] X. Zhang, H. Hao, Y. Shi, and J. Cui, "The mechanical properties of Polyvinyl Butyral (PVB) at high strain rates," Construction and Building Materials, vol. 93, pp. 404-415, Sep. 2015, doi: 10.1016/j.conbuildmat.2015.04.057.

[76] Glass in Buildings - Selection and Installation. AS 1288:2021. NSW, Sydney: Standards Association of Australia, 2021.

[77] Standard Guide for Structural Sealant Glazing. ASTM C1401-23. West Conshohocken, Pennsylvania, United States: ASTM International, 2023, doi: 10.1520/C1401-23.

[78] Standard Guide for Use of Silicone Sealants for Protective Glazing Systems. ASTM C1564-24. West Conshohocken, Pennsylvania, United States: ASTM International, 2024, doi: 10.1520/C1564-20R24.

[79] X. Wang, Y. Meng, J. Yang, X. Huang, F. Wang, and H. Xu, "Optimal kernel extreme learning machine model for predicting the fracture state and impact response of laminated glass panels," Thin-Walled Structures, vol. 162, May 2021, doi: 10.1016/j.tws.2021.107541.

[80] Standard Specification for Laminated Architectural Flat Glass. ASTM C1172-24. West Conshohocken, Pennsylvania, United States: ASTM International, 2024, doi: 10.1520/C1172-24

[81] F. J. Masters, K. R. Gurley, N. Shah, and G. Fernandez, "The vulnerability of residential window glass to lightweight windborne debris," Engineering Structures, vol. 32, no. 4, pp. 911-921, Apr. 2010, doi: 10.1016/j.engstruct.2009.12.016.